Geosci. Model Dev. Discuss., https://doi.org/10.5194/gmd-2017-175
Manuscript under review for journal Geosci. Model Dev.
Discussion started: 4 August 2017

Geoscientific Model Development Discussions

The SPACE 1.0 model: A Landlab component for 2-D calculation of sediment transport, bedrock erosion, and landscape evolution

Charles M. Shobe[1], Gregory E. Tucker[1], and Katherine R. Barnhart[1]

[1]CIRES and Department of Geological Sciences, University of Colorado

Correspondence to: Charles M. Shobe (charles.shobe@colorado.edu)

Abstract. Models of landscape evolution by river erosion are often either transport-limited (sediment is always available, but may or may not be transportable) or detachment-limited (sediment must be detached from the bed, but is then always transportable). While several models incorporate elements of, or transition between, transport-limited and detachment-limited behavior, most require that either sediment or bedrock, but not both, are eroded at any given time. We present SPACE (Stream Power with Alluvium Conservation and Entrainment) 1.0, a new model for simultaneous evolution of an alluvium layer and a bedrock bed based on conservation of sediment mass both on the bed and in the water column. The model treats sediment transport and bedrock erosion simultaneously, embracing the reality that many rivers (even those commonly defined as "bedrock" rivers) flow over a partially alluviated bed. The SPACE model is a component of the Landlab modeling toolkit, a Python-language library used to create models of earth surface processes. Landlab allows efficient coupling between the SPACE model and components simulating basin hydrology, hillslope evolution, weathering, lithospheric flexure, and other surface processes. Here, we first derive the governing equations of the SPACE model from existing sediment transport and bedrock erosion formulations and explore the behavior of local analytical solutions for sediment flux and alluvium thickness. We derive steady-state analytical solutions for channel slope, alluvium thickness, and sediment flux, and show that SPACE matches predicted behavior in detachment-limited, transport-limited, and mixed conditions. We provide an example of landscape evolution modeling in which SPACE is coupled with hillslope diffusion, and demonstrate that SPACE provides an effective framework for simultaneously modeling 2-D sediment transport and bedrock erosion.

1 Introduction

Rivers are the primary agents of land-surface lowering in non-glaciated landscapes (e.g., Whipple, 2004), and processes of erosion and sediment transport in rivers influence human river management (e.g., Graf et al., 2010), landscape mass balance (e.g., Armitage et al., 2011), and global biogeochemical cycling (e.g., Hilton, 2017). Interest in the effects of river channel evolution on landscape change over all spatial and temporal scales has led to the widespread proliferation of numerical models for channel evolution. Specifically within the landscape evolution community, many models have emerged to address the problem of river incision into sediment and bedrock over long timescales. River incision models fall into three broad categories. Transport-limited models (e.g., Willgoose et al., 1991) assume that erosion is limited by the capacity of a river to transport sediment or rock, but that an infinite supply of readily transportable material is available. In these models, elevation change in

Geosci. Model Dev. Discuss., https://doi.org/10.5194/gmd-2017-175
Manuscript under review for journal Geosci. Model Dev.
Discussion started: 4 August 2017

Geoscientific Model Development Discussions

the channel is set by the divergence of sediment transport capacity (e.g., Paola and Voller, 2005). Detachment-limited models assume that erosion is limited by a river's ability to remove sediment or rock from the bed, but that all detached material is transportable. While the underlying assumptions of these two end-member models differ, they produce identical steady-state longitudinal profiles (e.g., Whipple and Tucker, 2002; Lague et al., 2003). Further, as noted by Davy and Lague (2009), the superiority of one model over the other in tests against real landscapes appears to depend on the characteristics of test sites and on the comparison methods (e.g., Stock and Montgomery, 1999; Snyder et al., 2003; Tomkin et al., 2003; van der Beek and Bishop, 2003; Valla et al., 2010; Hobley et al., 2011). No simple detachment-limited or transport-limited model has been shown to agree with field data in a wide variety of natural settings, likely due in large part to the potential for both types of behavior to occur simultaneously. The third class of river erosion models, referred to here as "hybrid" models, attempts to incorporate aspects of both transport- and detachment-limited systems in order to achieve better agreement with field data and natural landscapes.

In this paper, we briefly review existing models that incorporate both sediment transport and bedrock erosion, and argue that many models are fundamentally limited by an inability to simultaneously transport sediment and erode bedrock. We then describe the SPACE 1.0 model, a new framework for modeling sediment transport and bedrock erosion at landscape evolution timescales. SPACE calculates sediment transport and bedrock erosion simultaneously, a capability not shared by many existing river erosion models. We show that the SPACE model transitions smoothly between transport-limited, detachment-limited, and mixed behavior, and that it matches analytical solutions for channel slope, sediment layer thickness, and sediment flux. Finally, we show that as a component of the Landlab toolkit, SPACE may be coupled with other landscape evolution model components for simple, efficient modeling of landscape change over long timescales.

2 Overview of hybrid river incision models

Perhaps the simplest parameterization of the influence of sediment on bedrock erosion is found in sediment-flux-dependent river incision models. Sediment-flux-dependent models form a class of detachment-limited model in which the interaction of sediment flux with sediment transport capacity enhances or inhibits bedrock erosion (e.g., Beaumont et al., 1992; Sklar and Dietrich, 1998; Whipple and Tucker, 2002; Sklar and Dietrich, 2004; Gasparini et al., 2006, 2007; Turowski et al., 2007; Hobley et al., 2011). Depending on the specific model formulation used, sediment may act as "cover," inhibiting bedrock erosion, or as "tools," accelerating bedrock erosion (see review in Hobley et al. (2011)). In most sediment-flux dependent models, erosion is influenced by a factor $f(q_s, q_c)$ ranging between 0 and 1, where q_s is sediment flux (either volume or mass flux per unit width) and q_c is sediment transport capacity. The value of $f(q_s, q_c)$ for any particular q_s and q_c depends on the choice of function f; proposed forms include a linear decline ($f(q_s, q_c) = 1 - \frac{q_s}{q_c}$; Beaumont et al. (1992)), parabola (Sklar and Dietrich, 2004), near-parabola (Gasparini et al., 2006), and other similar shapes (Turowski et al., 2007). The chief disadvantage of those sediment-flux-dependent incision models that do not also incorporate explicit sediment deposition is that using $f(q_s, q_c)$ as a proxy for the sediment influence on bedrock erosion precludes modeling of fully alluviated reaches (i.e., the river bed is simply vertically immobile when $f(q_s, q_c) = 0$). Once the bed is fully covered, these models cannot adjust their slope in response to

Geosci. Model Dev. Discuss., https://doi.org/10.5194/gmd-2017-175
Manuscript under review for journal Geosci. Model Dev.
Discussion started: 4 August 2017

additional sediment inputs (because they cannot model deposition). Sediment-flux-dependent incision models therefore require additional deposition components to treat rivers that may periodically become fully alluviated, including most channels on earth when considered over sufficiently long timescales.

Two potential solutions to the inflexibility of sediment-flux-dependent detachment-limited models have been proposed: "erosion-deposition" models and models with layers for multiple substrates. Erosion-deposition models (or under-capacity models), which explicitly treat simultaneous erosion and deposition of a substrate (Beaumont et al., 1992; Braun and Sambridge, 1997; Coulthard et al., 2002; Davy and Lague, 2009), may dynamically transition between transport-limited and detachment-limited behavior (see discussion in Davy and Lague (2009)). Davy and Lague (2009) present such a model based on the relative influence of erosion from the bed into the water column (erosion flux) and deposition from the water column onto the bed (deposition flux). When the deposition flux is much smaller than the erosion flux and the sediment transport length scale is long, their model becomes equivalent to a basic detachment-limited model. When the deposition flux increases and the transport length scale is short, the model predicts transport-limited behavior in which sediment flux divergence controls the channel bed elevation. The erosion-deposition framework, validated by the laboratory experiments of Lajeunesse et al. (2017), is capable of matching transient and steady-state longitudinal profile predictions made by both detachment-limited and transport-limited models, and smoothly transitions between the two types of model behavior (Davy and Lague, 2009). The model of Davy and Lague (2009) improved on previous under-capacity models by using a sediment transport length scale that scaled with water discharge. Importantly, models like the erosion-deposition model that transition between detachment-limited and transport-limited behavior allow the exploration of both types of models, and intermediate cases, with simple parameter changes rather than changes to the model structure. The major limitation of erosion-deposition models in their basic form is that they are derived for one material of constant erodibility, and thus are limited to eroding a single substrate (i.e., sediment or bedrock, but not both) at any given position and time. Without substantial modification, erosion-deposition models are therefore unable to compute simultaneous entrainment and erosion in mixed bedrock-alluvial systems.

To circumvent the single-substrate limitation discussed above, many models use a layer system in which an alluvium layer overlies bedrock in the channel (e.g., Tucker et al., 2001). The alluvium layer is generally treated with transport-limited rules, while the bedrock layer is treated as detachment-limited. Alternatively, Carretier et al. (2016) showed that a single erosion-deposition formulation may be applied for two or more distinct layers by varying the relevant erodibility parameter between layers (i.e., different erodibility for sediment than for bedrock) and explicitly partitioning the model timestep such that any time used to erode an overlying layer is not used to erode the next layer down. The fundamental limitation of such layer-based models is that they do not allow simultaneous evolution of the sediment layer and the underlying bedrock, making the implicit assumption that any small quantity of sediment fully covers the bed and inhibits bedrock erosion. Layer-based models, even when using the flexible erosion-deposition framework, are limited to eroding and depositing a single substrate at any given time. This is a significant simplification given the ubiquity of bedrock-alluvial channels on earth (Lague, 2010) and the frequently-observed transition between exposed bedrock in channel headwaters and sediment-mantled lowland reaches.

At least two models exist that have circumvented the problem of conventional layer-based models and allow simultaneous sediment and bedrock evolution. Lague (2010) explicitly tracked a layer of alluvium of thickness T_s with median grain size

Geosci. Model Dev. Discuss., https://doi.org/10.5194/gmd-2017-175
Manuscript under review for journal Geosci. Model Dev.
Discussion started: 4 August 2017

D_{50}. In his model, the bed is fully covered when $T_s/D_{50} > 1$, and bedrock is increasingly exposed (either linearly or exponentially) as T_s approaches zero. Zhang et al. (2015) followed a similar approach, expanding the saltation-abrasion model of Sklar and Dietrich (2004) to explicitly include local sediment transport dynamics rather than using a sediment-flux-dependent parameterization. Zhang et al. (2015) tracked the thickness of a sediment layer and compareed it to the macro-roughness of the bedrock surface such that alluvial thickness less than the macro-roughness length-scale results in exposed bedrock. Their geometric approach follows that of Lague (2010), but the Zhang et al. (2015) model incorporates both tools and cover effects due to its derivation from the saltation-abrasion model (Sklar and Dietrich, 2004).

We present a new model for simultaneous sediment and bedrock evolution that extends from the approaches of Davy and Lague (2009), Lague (2010), and Zhang et al. (2015). The Stream Power with Alluvium Conservation and Entrainment (SPACE) model is an erosion-deposition model in the style of Davy and Lague (2009). It incorporates progressive bedrock exposure with thinning of an alluvial layer in a similar way to Lague (2010) and Zhang et al. (2015) such that evolution of the alluvium and the bedrock may be simultaneously calculated. SPACE is unique in that it employs local analytical solutions for sediment flux changes in space and alluvium thickness changes in time made possible by combining expressions for conservation of sediment in the water column (e.g., Davy and Lague, 2009), conservation of sediment on the channel bed, and conservation of mass of bedrock. Our new model is a significant advance over layer-based models that cannot simultaneously erode both sediment and bedrock, as well as over sediment-flux-dependent river incision models in which sediment transport and storage is not treated explicitly. The SPACE model is designed to run over large spatial and temporal scales in two dimensions, and can be easily coupled to many other surface process models as part of the Landlab modeling toolkit. To maintain ease of model coupling and a relatively low level of complexity, we neglect some processes treated in previous models. Because sediment cover and transport are averaged across a model cell, we do not explicitly model the spatial distribution of sediment cover within a cell, or the entrainment and deposition of individual sediment grains (e.g., Hodge et al., 2011; Hodge and Hoey, 2012; Hodge, 2017). We do not employ dynamic channel width variations as in the models of Davy and Lague (2009), Lague (2010), and Coulthard et al. (2013), instead relying on empirical parameterizations of channel width as a function of drainage area or discharge. We also do not model the potential driving of bedrock erosion by bedload sediment (the tools effect), as used in Sklar and Dietrich (2004), Zhang et al. (2015), and other saltation-abrasion type models. Both width dynamics and bedload abrasion could be incorporated without changing the underlying model structure, but have been omitted in order to facilitate numerical model comparison to analytical solutions. Below we develop the SPACE model, verify our numerical solutions against analytical solutions, and show that SPACE can transition naturally between transport-limited and detachment-limited behavior. We briefly describe the Landlab modeling toolkit, and show an example landscape evolution model in which SPACE is coupled to other surface process models. The SPACE model marks a significant improvement on "tools and cover" and "sediment flux-dependent" river incision models in that bed sediment thickness is explicitly incorporated as a state variable, rather than relying on a cover fraction factor that is cast as a function of the relationship between sediment flux and sediment transport capacity. The model also improves upon previous models that include bedrock and alluvium layers, as it incorporates the reality that sediment entrainment, deposition, and bedrock erosion often happen simultaneously in mixed bedrock-alluvial channels.

Geosci. Model Dev. Discuss., https://doi.org/10.5194/gmd-2017-175
Manuscript under review for journal Geosci. Model Dev.
Discussion started: 4 August 2017

Geoscientific Model Development Discussions

3 SPACE model development

The SPACE model, like other erosion-deposition models, arises from sediment mass conservation in the water column (e.g., Davy and Lague, 2009) and on the channel bed. We consider a river bed that may vary dynamically in its degree of alluvial cover versus exposed bedrock, with a bedrock surface of height R, bed sediment of mean thickness H (the channel bed elevation η is therefore $R+H$), and water of mean flow depth h (Fig. 1). We use the term "SPACE model" to refer to the model equations, and "SPACE 1.0 component" to refer specifically to the numerical implementation of the SPACE model as a Landlab component.

3.1 Conservation of sediment in the water column

Davy and Lague (2009) showed that the rate of change in the volume of sediment in the water column per unit area of river bed $\frac{\partial (c_s h)}{\partial t}$ may be written as:

$$\frac{\partial (c_s h)}{\partial t} = E_s - D_s - \frac{\partial (Q_s/w)}{\partial x}, \tag{1}$$

where c_s is the concentration of sediment in the water column calculated by Q_s/Q (where Q is volumetric water discharge), E_s is the volumetric erosion flux of sediment per unit bed area, D_s is the volumetric deposition flux of sediment per unit bed area, Q_s is sediment flux in units of L^3/T, and w is channel width. Eq. (1) is sufficient when considering a channel bed on which only a single material (i.e., sediment) is exposed. Yet many channels are partially alluviated, indicating that sediment and bedrock may be eroded and entrained into the water column simultaneously. Such a scenario requires an addition to Eq. (1) to account for entrainment of bedrock material into the water column:

$$\frac{\partial (c_s h)}{\partial t} = E_s + (1 - F_f) E_r - D_s - \frac{\partial (Q_s/w)}{\partial x}. \tag{2}$$

E_r is the volumetric erosion flux of bedrock per unit bed area. F_f is a unitless fraction of fine sediment. F_f represents the volumetric fraction of bedrock that breaks into sediment small enough to be considered permanently in suspension, for which no further treatment of bed–water column interactions is needed. For bedrock that breaks only into sand and gravel fractions, F_f would be zero. Therefore, bed sediment thickness H and sediment flux Q_s only include sediment coarse enough that it does not enter permanent suspension. Assuming that $\frac{\partial (c_s h)}{\partial t} = 0$ (an important model assumption that potentially restricts applicability to hydrograph-scale modeling), the spatial gradient in sediment flux is a balance between sediment entrainment, rock erosion, and sediment deposition:

$$\frac{\mathrm{d} (Q_s/w)}{\mathrm{d}x} = E_s + (1 - F_f) E_r - D_s. \tag{3}$$

3.2 Conservation of sediment and rock on the channel bed

Change of channel bed elevation with time is the sum of changes in rock height and sediment thickness:

$$\frac{\partial \eta}{\partial t} = \frac{\partial R}{\partial t} + \frac{\partial H}{\partial t}. \tag{4}$$

Geosci. Model Dev. Discuss., https://doi.org/10.5194/gmd-2017-175
Manuscript under review for journal Geosci. Model Dev.
Discussion started: 4 August 2017

Following Eq. (4) and Davy and Lague (2009), conservation of sediment on the channel bed with sediment thickness H may be written as

$$\frac{\partial H}{\partial t} = \frac{D_s - E_s}{1 - \phi}, \tag{5}$$

where ϕ is the porosity of the bed sediment. Because there is no deposition of bedrock, the rate of change of bedrock elevation R over time is

$$\frac{\partial R}{\partial t} = U - E_r \tag{6}$$

where U is the rock uplift rate relative to baselevel. For simplicity we assume that the porosity of rock is zero, but rock porosity could easily be added to Eq. (6). Steady sediment thickness requires equal erosion and deposition of sediment $(D_s = E_s)$ and steady bedrock elevation requires that erosion of rock is balanced by rock uplift relative to baselevel $(U = E_r)$. Figure 1 shows a schematic of a model cell and defines relevant variables.

3.3 Erosion and entrainment of bed sediment and bedrock

As discussed in Davy and Lague (2009), any number of accepted expressions for entrainment of bed sediment and erosion of bedrock could be used for E_s and E_r, respectively. We consider here the unit stream power formulation in which entrainment and erosion are functions of water flux and slope (Howard, 1994; Whipple and Tucker, 1999). We add to the unit stream power model a means by which the flow may simultaneously entrain sediment and erode bedrock, and by which the bed may smoothly transition from fully alluviated to bare bedrock. Consider that the volumetric entrainment rate per unit bed area of bed sediment depends on unit stream power, but is also influenced by sediment thickness H relative to a reach-scale bedrock roughness length scale H_*. At low H/H_*, the lower points on the bedrock bed are mantled with sediment, but high points on the bedrock surface are still exposed. At high H/H_*, all areas of the bed are covered with sediment. Further, E_s must be zero when H is zero and no sediment is available to be entrained, and E_s must reach a maximum (for a given stream power) when there is enough sediment to fully cover the bed (Fig. 2). This approach is conceptually similar to the models of Lague (2010) (his exponential model) and Zhang et al. (2015), and similarly eliminates the need to explicitly track bedrock exposure. Given the conceptual model described above, the entrainment rate of sediment E_s may be written as:

$$E_s = (K_s q S^n - \omega_{cs}) \left(1 - e^{-H/H_*}\right), \tag{7}$$

where K_s is the sediment erodibility parameter, S is channel-bed slope, and n is a scaling exponent. q is water discharge per unit channel width, and may be calculated by any number of methods, the simplest being $q = A^m$ where A is drainage area and m is a scaling exponent (generally ≈ 0.5) designed to reflect downstream width changes (Leopold and Maddock, 1953). Using $q = A^m$ results in K_s and rock erodibility parameter K_r having dimensions of $\left[T^{-1}\right]$, but dimensions vary based on which parameterization for q is used (in the general case of q being volumetric water flux per unit width, K_s and K_r have dimensions of $\left[L^{-1}\right]$). ω_{cs} is a threshold stream power required for sediment entrainment. In very simple cases ω_{cs} may be neglected,

Geosci. Model Dev. Discuss., https://doi.org/10.5194/gmd-2017-175
Manuscript under review for journal Geosci. Model Dev.
Discussion started: 4 August 2017

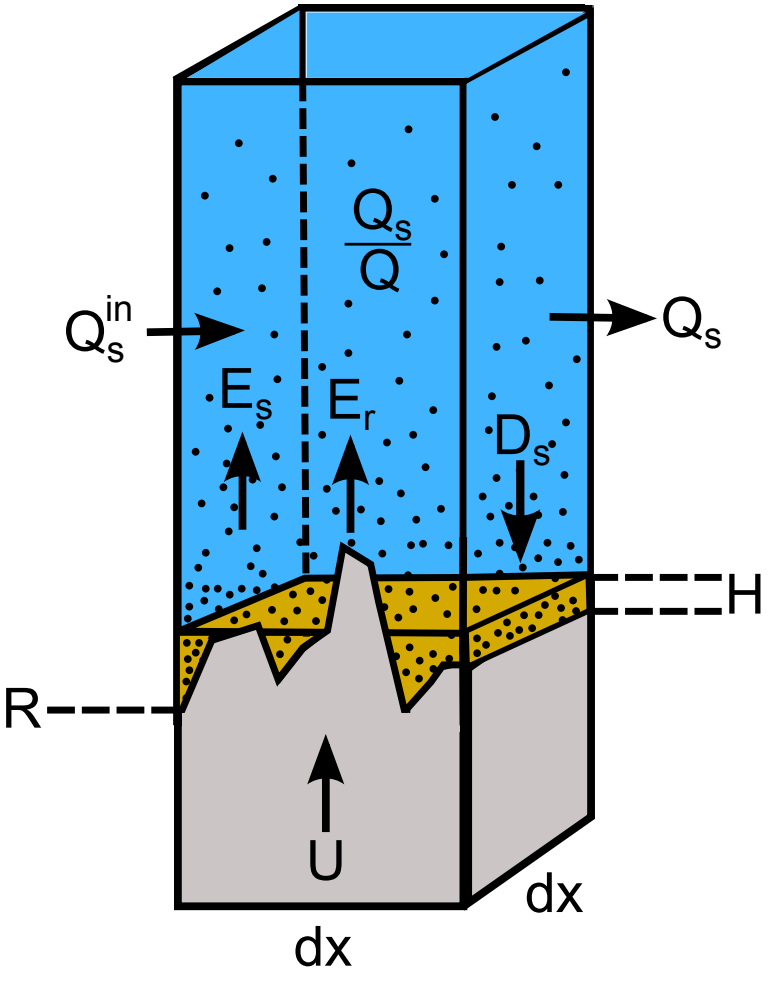

Figure 1. Conceptual sketch of a single model cell and definition of variables. Rock surface elevation R is defined as the elevation of the lowest point on the bedrock surface, and is also used as the lower boundary for the thickness H of the alluvial layer.

but the ability to include a threshold term is important in any river evolution model as threshold effects have been shown to significantly alter model outcomes (Snyder et al., 2003; Tucker, 2004; Lague et al., 2005; DiBiase and Whipple, 2011).

If sediment entrainment declines with decreasing sediment thickness as a result of increased bedrock exposure, bedrock erosion should follow an inverse but conceptually similar pattern (Fig. 2). Assuming that increasing mean sediment thickness leads to higher proportions of bedrock covered by sediment and that sediment cover inhibits erosion (e.g., Beaumont et al., 1992; Whipple and Tucker, 2002; Sklar and Dietrich, 2004; Gasparini et al., 2006, 2007; Turowski et al., 2007; Hobley et al., 2011), the volumetric erosion rate of bedrock per unit bed area may be written as

$$E_r = (K_r q S^n - \omega_{cr})\, e^{-H/H_*}. \tag{8}$$

Geosci. Model Dev. Discuss., https://doi.org/10.5194/gmd-2017-175
Manuscript under review for journal Geosci. Model Dev.
Discussion started: 4 August 2017

Geoscientific Model Development Discussions

Here, K_r is the bedrock erodibility parameter, which is generally expected to be substantially lower than K_s. ω_{cr} is the threshold stream power for detachment of bedrock, which may vary significantly depending on the relative dominance of plucking or abrasion (e.g., Hancock et al., 1998; Whipple et al., 2000) as well as the weathered state of the bedrock (Hancock et al., 2011; Johnson and Finnegan, 2015; Small et al., 2015; Murphy et al., 2016; Shobe et al., 2017). Eq. (8) falls into the category of "cover" models, which treat erosion reduction by sediment shielding the bed without incorporating the potential erosive effects of mobile sediment (e.g., Beaumont et al., 1992; Lague, 2010; Shobe et al., 2016). The smooth transitions between bare-bedrock, bedrock-alluvial, and fully alluviated channels given by Eq. (7 and 8) are both more stable and more realistic than models in which the existence of any alluvium fully covers the bedrock (implying a perfectly smooth, planar bedrock surface). Figure 2 shows the pattern of sediment entrainment and bedrock erosion over different values of H/H_*. $f\left(H/H_*\right)$ in Fig. 2 is the dimensionless exposure term that modifies stream power entrainment and erosion in Eq. (7 and 8) (i.e., e^{-H/H_*} or $\left(1-e^{-H/H_*}\right)$). Perhaps the most significant simplification in our model is that we do not include explicit treatment of the erosive effects of grains in transport (e.g., Sklar and Dietrich, 1998, 2001, 2004; Gasparini et al., 2006; Turowski et al., 2007; Lamb et al., 2008; Cook et al., 2013). Such an effect could enhance sediment entrainment if grains in saltation hit resting grains and enabled their entrainment, and could enhance bedrock erosion if sediment-rich water were flowing over well-exposed bedrock. We assume for the purposes of model validation against analytical solutions that these effects are negligible relative to changes in unit stream power and bed cover. The major advantages of the exponential entrainment and erosion approach outlined here are that 1) sediment and bedrock may be simultaneously entrained/eroded into the water column, 2) the presence of sediment does not completely inhibit bedrock erosion at low values of H/H_*, which is supported by modeling and observations of mixed bedrock-alluvial channels (Johnson et al., 2009; Johnson, 2014; Ferguson et al., 2017; Hodge, 2017) and 3) model stability is improved because sediment thickness gradually approaches zero, preventing a sudden transition from sediment entrainment to bedrock erosion. Many different rules for sediment entrainment and bedrock erosion could be used in this model framework in place of stream-power type equations. No matter how erosive power is calculated, the SPACE approach allows both erodibility and entrainment/detachment thresholds to be chosen independently for sediment and bedrock, unlike in strict detachment/transport limited models or the basic form of erosion-deposition models. This enables the treatment of systems with multiple erosion thresholds, such as a river for which bedrock erosion requires both mobilization of an alluvial cover (described by ω_{cs}) and the plucking of bedrock blocks (described by ω_{cr}).

3.3.1 Optional smoothing of entrainment/erosion thresholds

The approach outlined above allows for the incorporation of an entrainment threshold for sediment and an erosion threshold for bedrock such that entrainment/erosion is zero when stream power is below the chosen threshold(s). Erosion thresholds representing a sharp transition between no erosion (below threshold) and erosion (above threshold) have a long history in fluvial erosion modeling (e.g., Snyder et al., 2003; Tucker, 2004; Lague et al., 2005; DiBiase and Whipple, 2011). With a sharp or discontinuous erosion threshold, the transition from no erosion to erosion is abrupt. However, recent work has shown that entrainment thresholds for sediment may be a state function of grain size distribution, bed sorting, sediment flux, hydraulic conditions, and flow history (see review in Johnson (2016)), and that bedrock erodibility can depend on the rock

Geosci. Model Dev. Discuss., https://doi.org/10.5194/gmd-2017-175
Manuscript under review for journal Geosci. Model Dev.
Discussion started: 4 August 2017

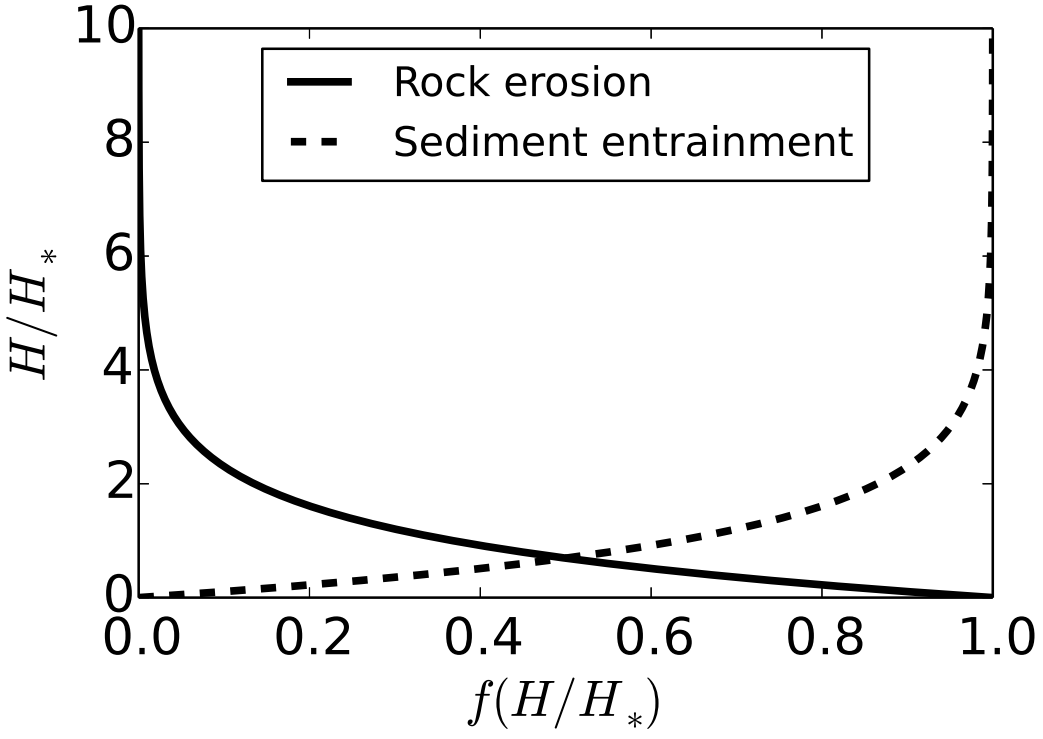

Figure 2. Dimensionless efficiency of erosion and deposition ($f(H/H_*)$) for different values of H/H_*. Erosive power is multiplied by $f(H/H_*)$ in the model to account for the relative exposure of sediment and bedrock. Such a formulation accounts for the fact that bedrock beds are rough, and low points may become sediment-mantled while high points remain exposed (e.g., Johnson, 2014; Zhang et al., 2015). H_* is therefore a length scale representing reach-scale bedrock roughness. Sediment entrainment for a given stream power increases with increasing H/H_*, while bedrock erosion declines as a response to sediment mantling of the bed. At values of $H/H_* \approx 6$, all bed lowering is driven by sediment entrainment and bedrock erosion is negligible. This heuristic representation of mixed alluvial-bedrock channel dynamics is conceptually similar to the approaches taken by Lague (2010) and Zhang et al. (2015).

inundation history and therefore the historic hydrograph (Hancock et al., 2011; Small et al., 2015; Shobe et al., 2017). Further, in numerical modeling in general, the use of strict single-value thresholds can introduce discontinuities into model response functions, hindering sensitivity analysis and optimization procedures (Clark and Kavetski, 2010; Kavetski and Clark, 2010). While we do not attempt to treat the specific processes responsible for altering entrainment and erosion thresholds, we include an optional exponential expression for threshold stream power such that entrainment/erosion does not go to zero when stream power ω equals the threshold value ω_c, but declines exponentially as ω/ω_c declines. The threshold stream power is expected to be different for rock than for sediment, with ω_{cr} likely being larger in most cases than ω_{cs}. In this formulation, the expressions for sediment entrainment and bedrock erosion (Eq. (7 and 8)) become:

$$E_s = \left(K_s q S^n - \omega_{cs}\left(1 - e^{-\omega/\omega_{cs}}\right)\right)\left(1 - e^{-H/H_*}\right) \tag{9}$$

Geosci. Model Dev. Discuss., https://doi.org/10.5194/gmd-2017-175
Manuscript under review for journal Geosci. Model Dev.
Discussion started: 4 August 2017

and

$$E_r = \left(K_r q S^n - \omega_{cr}\left(1 - e^{-\omega/\omega_{cr}}\right)\right) e^{-H/H_*}. \quad (10)$$

Inspection of Eq. (9 and 10) reveals that when $\omega \gg \omega_c$, the threshold term approaches ω_c, yielding behavior identical to single-value threshold models. When $\omega \ll \omega_c$, the threshold term approaches ω and the entrainment or erosion rate approaches zero. Evaluation of the full behavior of models using an exponentially declining threshold is beyond the scope of this paper, and the use of Eq. (9 and 10) is optional in the SPACE model. The smoothly declining threshold is recommended for applications involving analysis of the model response surface, or other situations in which sharp discontinuities in model responses could hinder analysis (Clark and Kavetski, 2010; Kavetski and Clark, 2010).

3.4 Deposition of sediment

The flux of sediment from the water column onto the bed is the product of sediment concentration averaged over the depth of the water column and effective sediment settling velocity V (Davy and Lague, 2009):

$$D_s = c_s V = \frac{Q_s}{Q} V. \quad (11)$$

V is not the still-water particle settling velocity, but is the net effective settling velocity after accounting for the upward effects of turbulence. V also incorporates the vertical gradient in sediment concentration through the water column (d^* in Davy and Lague (2009)). In an equivalent formulation, Davy and Lague (2009) treated the sediment deposition rate as $D_s = d^* c_s V$, where d^* is a dimensionless number that relates sediment concentration near the bed to mean sediment concentration in the water column.

3.5 Steady-state analytical solutions

We develop steady-state analytical solutions for sediment flux Q_s, channel slope S, and bed sediment thickness H, all of which are steady when $\frac{\partial (c_s h)}{\partial t} = 0$. We assume for the purposes of this derivation that there are no entrainment or erosion thresholds, and that F_f and ϕ are both negligible, assumptions that are easily relaxed. We define steady state in this system as a state of time-invariant bedrock elevation and topographic elevation (which also implies time-invariant sediment thickness). This occurs when two conditions are satisfied. First, rock uplift must be balanced by bedrock erosion such that

$$\frac{\partial R}{\partial t} = 0 = U - K_r q S^n e^{-H/H_*}. \quad (12)$$

Second, sediment entrainment and deposition must balance each other such that sediment thickness H is unchanging in time:

$$\frac{\partial H}{\partial t} = 0 = V \frac{Q_s}{Q} - K_s q S^n \left(1 - e^{-H/H_*}\right). \quad (13)$$

At steady state, the volumetric sediment flux Q_s at any point along the channel must balance the volume of newly uplifted rock in the area draining to that point:

$$Q_s = UA. \quad (14)$$

Geosci. Model Dev. Discuss., https://doi.org/10.5194/gmd-2017-175
Manuscript under review for journal Geosci. Model Dev.
Discussion started: 4 August 2017

To find steady state channel slope, we begin by rearranging Eq. (13) and combining with Eq. (14):

$$K_s q S^n \left(1 - e^{-H/H_*}\right) = V\frac{UA}{Q}. \tag{15}$$

Recognizing that $Q = Ar$ where r is a runoff rate per unit area:

$$K_s q S^n \left(1 - e^{-H/H_*}\right) = \frac{VU}{r}. \tag{16}$$

We rearrange Eq. (16) to isolate e^{-H/H_*}, substitute into Eq. (12) and solve for S to yield:

$$S = \left[\frac{UV}{K_s q r} + \frac{U}{K_r q}\right]^{1/n}, \tag{17}$$

or if $q = A^m$ as in the simple stream power formulation,

$$S = \left[\frac{UV}{K_s A^m r} + \frac{U}{K_r A^m}\right]^{1/n}. \tag{18}$$

When $n = 1$, the second term on the right-hand side is the slope predicted by a detachment-limited incision model in which slope increases with faster rock uplift, lower rock erodibility, or less water discharge (or drainage area). The first term on the right-hand side describes the additional component of slope required to transport sediment. That component of slope must increase with increasing settling velocity, lower sediment erodibility, and lower water discharge. Davy and Lague (2009) derived a similar expression for slope-discharge scaling for their erosion-deposition model. The major difference between our result and theirs is that their expression is for slope of a single bed material with a single bed erodibility when erosion balances rock uplift, whereas Eq. (18) incorporates equilibrium in both sediment thickness and bedrock height.

Solving Eq. (16) for H gives steady state bed sediment thickness as a function of channel slope:

$$H = -H_* \ln\left[1 - \frac{VU}{r K_s q S^n}\right]. \tag{19}$$

To obtain a slope-independent solution for H, we can combine Eq. (18 and 19) and simplify:

$$H = -H_* \ln\left[1 - \frac{V}{\frac{K_s r}{K_r} + V}\right]. \tag{20}$$

The SPACE model therefore predicts constant sediment thickness along the channel at steady state as long as all parameters in Eq. (20) are constant in space. As settling velocity becomes larger, $\frac{V}{\frac{K_s r}{K_r}+V}$ approaches one and H becomes large. As K_s increases and sediment is more easily entrained from the bed, $\frac{V}{\frac{K_s r}{K_r}+V}$ and therefore H both approach zero. Increasing bedrock erodibility K_r causes an increase in steady state H as more sediment is created from detached bedrock.

3.6 Dimensional analysis

We present a nondimensionalization of the model described above. For simplicity, we assume that sediment entrainment and bedrock erosion thresholds are negligible, though the model allows independent entrainment and erosion thresholds as shown

Geosci. Model Dev. Discuss., https://doi.org/10.5194/gmd-2017-175
Manuscript under review for journal Geosci. Model Dev.
Discussion started: 4 August 2017

above. The model contains three independent variables, Q_s, H, and R, the latter two of which are summed to give land surface elevation. Each of these variables requires a scale for nondimensionalization. We begin by nondimensionalizing sediment flux:

$$Q_s' = \frac{Q_s V}{K_s q^2 S w}. \tag{21}$$

Sediment thickness H and bedrock elevation R may both be scaled by the sediment layer length-scale H_*:

$$H' = H/H_* \tag{22}$$

and

$$R' = R/H_*, \tag{23}$$

and downstream distance x by the length scale q/V (noted by Davy and Lague (2009) and found to govern the transition between detachment-limited and transport-limited behavior):

$$x' = xV/q. \tag{24}$$

Finally, time t is nondimensionalized by:

$$t' = tV/H_*. \tag{25}$$

Replacing the dimensionless variables into the governing equations yields the following equations for dimensionless sediment flux, sediment thickness, and rock elevation, which are applicable for negligible erosion thresholds:

$$\frac{\mathrm{d}Q_s'}{\mathrm{d}x'} = S\left(1 - e^{-H'}\right) + (1 - F_f)\left[\frac{K_r}{K_s}\right] S e^{-H'} - Q_s' \tag{26}$$

$$\frac{\partial H'}{\partial t'} = \left[\frac{K_s q}{V}\right]\left(Q_s' - S\left(1 - e^{-H'}\right)\right) \tag{27}$$

$$\frac{\partial R'}{\partial t'} = \left[\frac{U}{V}\right] - \left[\frac{K_r}{K_s}\right]\left[\frac{K_s q}{V}\right] S e^{-H'}. \tag{28}$$

Three dimensionless parameters appear in Eq. (26–28): a ratio of erodibilities $\left[\frac{K_r}{K_s}\right]$, a sediment entrainment ratio $\left[\frac{K_s q}{V}\right]$, and a normalized rock uplift rate $\left[\frac{U}{V}\right]$. The erodibility ratio reflects the relative ease of eroding bedrock and entraining sediment, and is influenced in natural systems by bedrock and sediment lithology, grain size, and grain sorting on the channel bed. The sediment entrainment ratio encompasses competition between sediment entrainment, which is driven by high water discharge and high sediment erodibility, and sediment deposition, driven by high grain settling velocity. Notably, the sediment entrainment ratio contains the q/V length scale described by Davy and Lague (2009). The model predicts detachment-limited behavior when q/V, and therefore our entrainment ratio, are large, and transport-limited behavior when they are small. The normalized rock uplift rate shows the relative importance of rock uplift and grain settling velocity, with increases in both driving increased channel slope.

Geosci. Model Dev. Discuss., https://doi.org/10.5194/gmd-2017-175
Manuscript under review for journal Geosci. Model Dev.
Discussion started: 4 August 2017

4 Numerical implementation and local analytical solutions

In this section we describe the forward-time numerical solution of the SPACE model in two dimensions. The solution to the model equations in each timestep consists of three conceptual steps. First, sediment flux is calculated with a local analytical solution, described below, at every node working in order from upstream to downstream. Second, sediment thickness is calculated at every node using a local analytical solution for $H(t)$, which we develop below. Third, bedrock erosion is calculated for each node.

4.1 Calculation of sediment flux

As shown in Eq. (3), the x-directed rate of change in sediment flux depends on sediment entrainment, bedrock erosion, and sediment deposition. The dependence of deposition rate on $\frac{Q_s}{Q}$ means that the deposition flux, and therefore the change in sediment flux, at a given node depends on the sediment flux entering that node from upstream. It is therefore critical to order nodes in upstream to downstream order and calculate sediment flux iteratively from upstream to downstream. This approach unfortunately precludes simultaneous calculation of sediment flux at all nodes. Landlab's flow routing capabilities order all nodes into a "stack" following the methodology of Braun and Willett (2013). Because our sediment flux calculations must progress from upstream to downstream, we use their "inverted stack order" in which nodes are ordered from upstream to downstream, allowing the SPACE algorithm to efficiently sum water and sediment fluxes at tributary junctions. In addition, the downstream sediment flux calculation is written and compiled using the Cython library, giving it significant performance improvements over the same loop in pure Python.

Numerical integrations of sediment entrainment and deposition are often significant sources of model inaccuracy and instability due to the spatial extrapolation of linear entrainment and deposition equations. Consider a river reach of length $\mathrm{d}x$ with clear water entering the reach at the upstream end. The initial sediment entrainment rate is $E_s = K_s q S^n - \omega_{cs}$ and the initial deposition rate is zero because $Q_s = 0$. However, two natural processes make the linear extrapolation of these initial entrainment and deposition rates over cell length $\mathrm{d}x$ inappropriate. First, sediment entrainment rate may decline over x as sediment thickness H declines if H is not much greater than H_*. Second, as sediment is entrained over distance $\mathrm{d}x$, Q_s increases, which drives a progressive increase in deposition rate. Simply numerically integrating Eq. (3) to calculate sediment flux does not account for either the progressive decline in available sediment or the progressive saturation of the water column and increase in deposition flux. We have therefore developed a local analytical solution to account for such effects. This approach prevents severe overestimation of sediment entrainment into the water column, making SPACE more stable than models that do not account for within-cell changes in Q_s. Our local analytical solution for sediment flux accounts for the fact that sediment flux from upstream Q_s^{in} and any net erosion (or deposition) in a model cell of area $\mathrm{d}x^2$ contribute to Q_s, which drives deposition. Let Q_s^{out} represent the sum of sediment influx, erosion, and deposition such that Q_s^{out} is the net erosion rate in the cell multiplied by the cell area:

$$Q_s^{out} = Q_s^{in} + (1-\phi)\, E_s \mathrm{d}x^2 + (1-F_f)\, E_r \mathrm{d}x^2 - V\frac{Q_s}{rA}. \tag{29}$$

Geosci. Model Dev. Discuss., https://doi.org/10.5194/gmd-2017-175
Manuscript under review for journal Geosci. Model Dev.
Discussion started: 4 August 2017

Geoscientific Model Development Discussions

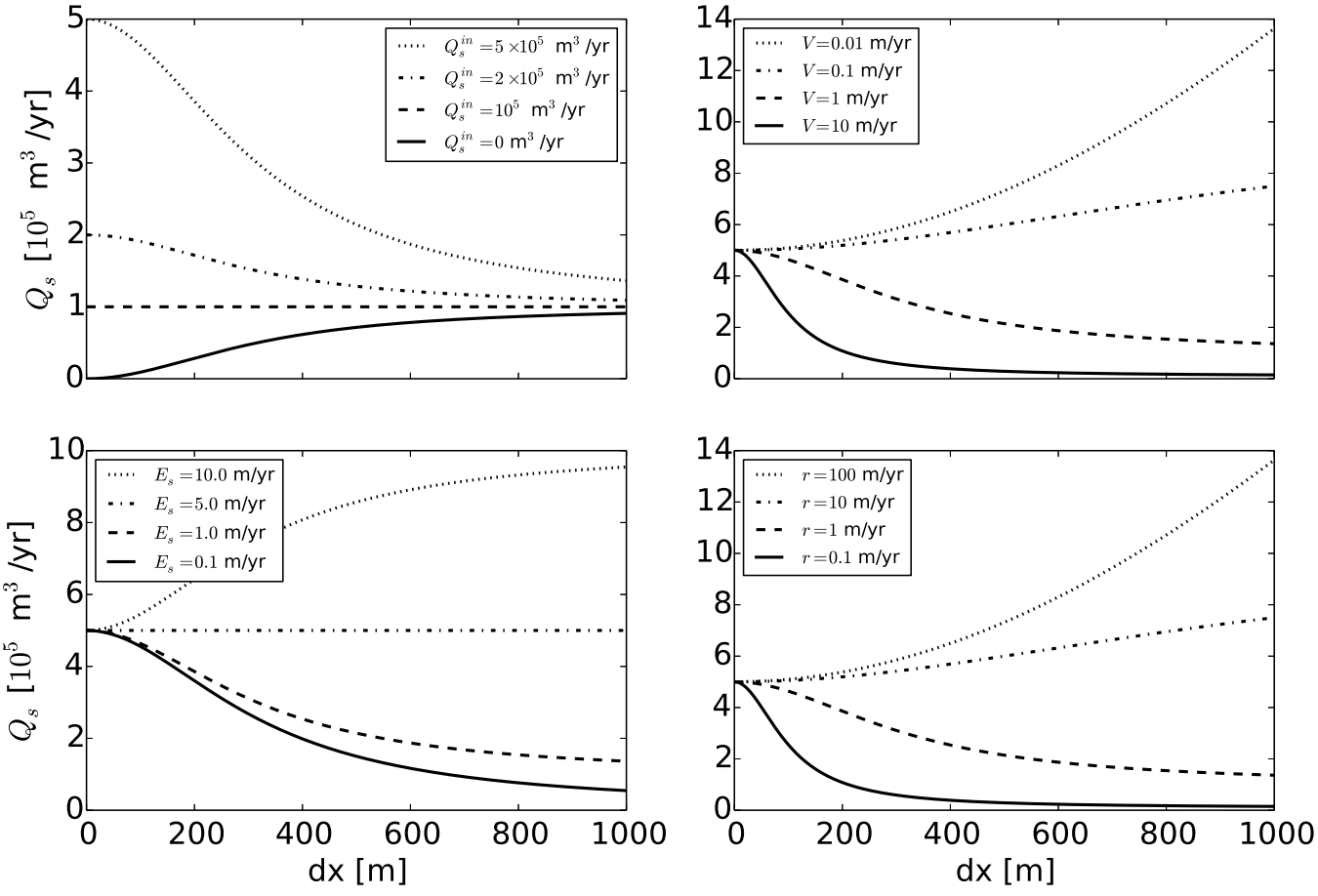

Figure 3. Sediment flux Q_s as a function of distance $\mathrm{d}x$ as calculated by the local analytical solution (Eq. (30)) at a given drainage area ($A = 10^5$ m^2). In each panel, one parameter is varied while all others are held constant. The sediment flux coming in from upstream is an important control on Q_s at short length scales, but declines in importance as $\mathrm{d}x$ approaches 1000 m. High values of settling velocity cause low Q_s and vice versa. High sediment entrainment rates lead to high Q_s as do high runoff rates. Parameter values (except where changed in the four panels) are: $Q_s^{in} = 50{,}000$ m^3/yr, $V = 1.0$ m/yr, $E_s = 1.0$ m/yr, and $r = 1.0$ m/yr. $E_r = 0$ and $\phi = 0$ for simplicity in this case.

If we use $Q_s = Q_s^{out}$ for the deposition term (last term on the right hand side), equation 29 may then be solved for Q_s to yield the local analytical solution for Q_s within a model cell:

$$Q_s^{out} = \frac{Q_s^{\mathrm{in}} + (1-\phi)\,E_s \mathrm{d}x^2 + (1-F_f)\,E_r \mathrm{d}x^2}{1 + V\mathrm{d}x^2/(rA)}. \tag{30}$$

Eq. (30) breaks down where $rA = 0$, which is acceptable because Q_s will always be zero where $rA = 0$. Figure 3 shows Q_s as a function of some of the relevant variables in Eq. (30).

Geosci. Model Dev. Discuss., https://doi.org/10.5194/gmd-2017-175
Manuscript under review for journal Geosci. Model Dev.
Discussion started: 4 August 2017

Geoscientific Model Development Discussions

4.2 Calculation of sediment thickness

After calculation of Q_s at every node, sediment thickness $H(t)$ is calculated according to Eq. (5). Similar to the solution of the sediment flux equation, solution of $H(t)$ is subject to numerical inaccuracies and instabilities driven by the dependence of E_s on H. Extrapolating $\frac{\mathrm{d}H}{\mathrm{d}t}$ over a full timestep using H_0 (H at the beginning of the timestep) causes overestimation of sediment entrainment, especially at larger timesteps. We therefore develop a local analytical solution for $H(t)$ for a small time interval over which variations in H are important but D_s, K_s q, and S (as well as any entrainment threshold) may be considered steady. We find the analytical solution for $H(t)$ by integrating Eq. (5) with respect to time with the knowledge that H has some initial value H_0 at the beginning of a timestep ($t = 0$):

$$H(t) = H_* \ln\left[\frac{1}{(D_s/(1-\phi))/\widehat{E}_s - 1}\left(e^{\left(D_s/(1-\phi)-\widehat{E}_s\right)t/H_*}\left(\left(\frac{(D_s/(1-\phi))}{\widehat{E}_s} - 1\right)e^{H_0/H_*} + 1\right) - 1\right)\right], \tag{31}$$

where

$$\widehat{E}_s = K_s q S^n - \omega_{cs}. \tag{32}$$

Inspection of Eq. (31) reveals that $H(t)$ may become undefined in two physically realistic situations. The first is where $(D_s/(1-\phi))/\widehat{E}_s = 1$ and the second is where $\widehat{E}_s = 0$. Eq. (31) is therefore only applied at nodes with $D_s/(1-\phi) \neq \widehat{E}_s$ and $\widehat{E}_s > 0$. When $D_s/(1-\phi) = \widehat{E}_s$, the change in alluvium thickness with time becomes $\frac{\mathrm{d}H}{\mathrm{d}t} = e^{-H/H_*}$. Integrating with respect to time and applying $H = H_0$ at $t = 0$ gives the solution for $H(t)$ when $D_s/(1-\phi) = \widehat{E}_s$:

$$H(t) = H_* \ln\left[\frac{K_s q S^n - \omega_{cs}}{H_*} t + e^{H_0/H_*}\right]. \tag{33}$$

When $\widehat{E}_s \leq 0$, no entrainment of sediment occurs and any changes in $H(t)$ are driven by deposition. In this case, changes in H are computed with a simple forward numerical solution:

$$H(t) = H_0 + \frac{D_s}{1-\phi}\mathrm{d}t. \tag{34}$$

In all cases, the relevant equation for $H(t)$ is solved each timestep using $t = \mathrm{d}t$ where $\mathrm{d}t$ is the model timestep length. Unlike for Q_s, H may be simultaneously calculated at every node, allowing efficient solution of Eq. (31–34) over the entire model domain. Figure 4 shows $H(t)$ as a function of some of the relevant variables in Eq. (31).

4.3 Calculation of change in bedrock height

Bedrock erosion is calculated by combining Eq. (6 and 8) and solving forward in time from a previous rock elevation R_0:

$$R = R_0 + \left(U - (K_r q S^n - \omega_{cr})\, e^{-H/H_*}\right)\mathrm{d}t. \tag{35}$$

The simple forward numerical solution employed in Eq. (35) becomes inappropriate at very large timesteps, as H may change significantly, influencing channel slopes and therefore bedrock erosion. However, because bedrock erosion is generally a much slower process than sediment entrainment in most cases, Eq. (35) is unlikely to introduce substantial instability.

Geosci. Model Dev. Discuss., https://doi.org/10.5194/gmd-2017-175
Manuscript under review for journal Geosci. Model Dev.
Discussion started: 4 August 2017

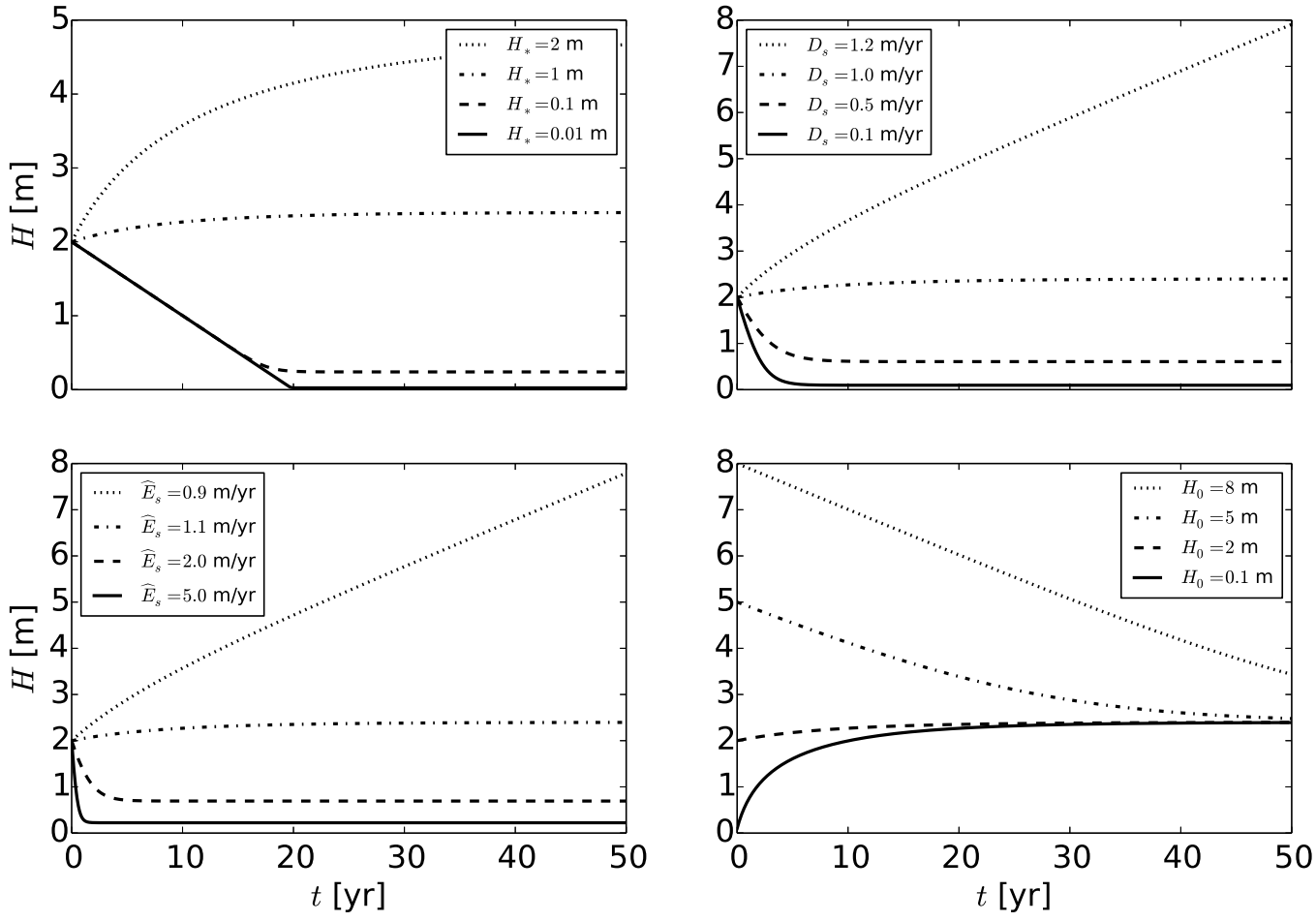

Figure 4. Bed sediment thickness H as a function of time as calculated by our local analytical solution (general case for $D_s/(1-\phi) \neq \widehat{E}_s$). In each panel, a single parameter in Eq. (31) is varied while all others are held constant. H_0, the initial sediment thickness, sets the initial value of the function. The value of H approached over long timescales is set by competition between the rates of sediment erosion and deposition, where higher sediment erosion rates drive bed sediment thickness down (lower left panel) and higher deposition rates result in greater bed sediment thickness (upper right panel). Except in cases where $D_s > E_s$, our local analytical solution converges on a constant value as $t \to \infty$. When $D_s > E_s$, the solution converges to a simple linear extrapolation of the deposition rate over time. Parameter values (except where changed in the four panels) are: $H_* = 1.0$ m, $D_s = 1.0$ m/yr, $\widehat{E}_s = 1.1$ m/yr (resulting in $E_s = 0.95$ m/yr when $H_0/H_* = 2$), and $H_0 = 2.0$ m/yr. $\phi = 0$ for simplicity in this case.

Geosci. Model Dev. Discuss., https://doi.org/10.5194/gmd-2017-175
Manuscript under review for journal Geosci. Model Dev.
Discussion started: 4 August 2017

5 Implementing SPACE in Landlab

5.1 Landlab modeling toolkit

Landlab is a flexible, open-source modeling framework written in Python that allows efficient model building and hypothesis testing across many subdisciplines in earth system science (Hobley et al., 2017). Landlab is a plug-and-play environment in which users can easily build two-dimensional numerical models consisting of any number of well-vetted components (e.g., Tucker et al., 2016; Adams et al., 2017) along with user-specific equations and functionality. The greatest advantages of using Landlab are 1) its built-in gridding engine, which creates model grids, efficiently stores spatially distributed variables, and handles boundary conditions, and 2) the ability to easily couple different components into a single model sharing a single grid. Landlab allows efficient coupling of components representing fluvial erosion, hillslope processes, basin hydrology (Adams et al., 2017), geodynamics, vegetation, and many other processes into novel surface dynamics models.

Landlab's gridding engine supports grids consisting of square and rectangular grids ("raster grids"), hexagonal grids, and Voronoi–Delaunay interlocked meshes (Hobley et al., 2017). Every Landlab grid is made up of nodes, cells, and links. Nodes are points in (x, y) space. Cells are polygons surrounding all non-boundary (interior) nodes that may be rectangular, hexagonal, or defined by Voronoi polygons depending on the chosen grid type. Links connect adjacent pairs of nodes and are directional. Rectangular grids have four links per node, hexagonal grids have six, and Voronoi grids have a number of links per node equivalent to the number of faces on each Voronoi polygon. Links have default directionality, but this directionality does not determine the directions of fluxes in Landlab models, which are set by gradients along links. In this paper, we focus for simplicity on a square ($\Delta x = \Delta y$) raster grid, which is currently the only grid type supported by the SPACE model. A diagram of a generic raster grid is shown in Fig. 5. Nodes, cells, and links may all store model data in the form of NumPy arrays associated with one of the three grid elements. Each data field is defined by a keyword in a dictionary data structure attached to a certain grid element. The SPACE model, for example, tracks sediment depth at all grid nodes, a field that may be accessed by any component (this field is called "soil depth" in Landlab to keep terminology standard between hillslope and fluvial components). An array of sediment depths at all grid nodes could be found by typing: *grid.at_node["soil__depth"]*. The treatment of boundary conditions in Landlab grids is described thoroughly by Hobley et al. (2017) and Adams et al. (2017). In short, nodes may be set as "boundary" nodes and then defined as open, fixed-gradient, or closed boundaries. Non-boundary nodes are set as "core" nodes.

6 Verification and evaluation: Comparison to analytical solutions for detachment-limited, transport-limited, and mixed cases

As discussed above, the SPACE model equations are capable of replicating both detachment-limited (when there is no sediment and $F_f = 1$) and transport-limited (when $H \gg H_*$) model behavior. In this section we compare the behavior of the SPACE 1.0 Landlab component (the numerical implementation of the SPACE model equations presented above) to steady-state analytical solutions for standard detachment-limited and transport-limited models to assess whether our numerical implementation of the

Geosci. Model Dev. Discuss., https://doi.org/10.5194/gmd-2017-175
Manuscript under review for journal Geosci. Model Dev.
Discussion started: 4 August 2017

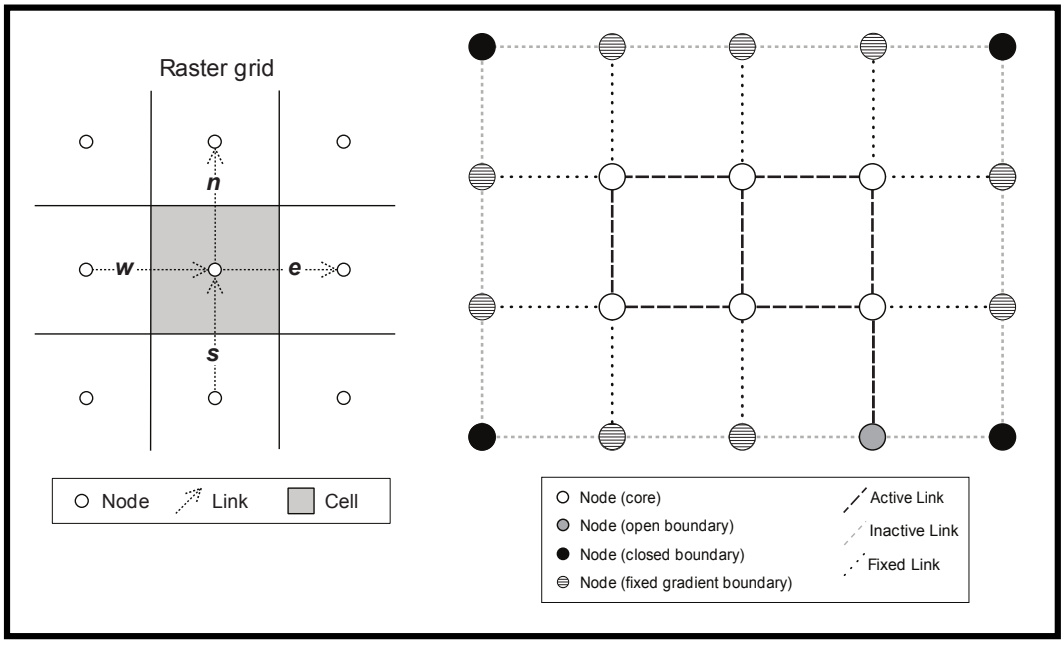

Figure 5. Left: the Landlab structured raster model grid, with definitions for major grid elements. State variables such as sediment depth and sediment flux are stored at grid nodes. While gradients such as topographic slope are calculated along links, the slope value representing the steepest descent from a node to its flow receiving neighbor is stored on the node itself. Link direction is topological; the direction of fluxes is set by gradients along links. Figure reproduced from Fig. 3 and 4 in Adams et al. (2017).

SPACE algorithm can replicate these two end-member cases. In addition, we test the performance of the SPACE component against steady-state analytical solutions for a mixed case where both bedrock erosion and sediment transport influence channel evolution. For the three test cases we use a simple 20 x 20 node square raster grid with $\mathrm{d}x = 100$ m, for a 2 km x 2 km model domain. The initial topography of the domain is a plane tilted to the lower-left (southwest) corner with random microscale roughness to force flow convergence. The lower-left corner is the only open boundary, and is therefore the basin outlet in all cases. Such a setup results in a model domain that drains to the single open boundary node, allowing predictable drainage network development. The random seed is held constant so that all runs start from the same initial topography. For simplicity in these test cases, there are no other surface process models (e.g., hillslope models) coupled to the SPACE component. We use a timestep of 1 year and run the model for 100,000 years for the detachment and transport limited comparisons, and 200,000 years for the mixed bedrock-alluvial comparison (see table 1). We define steady state as having been achieved when every interior (non-boundary) node is lowering at the same rate as the baselevel node to within 10^{-6} m/yr precision, but allow the model to run for the full imposed run time even after steady state has been achieved.

Geosci. Model Dev. Discuss., https://doi.org/10.5194/gmd-2017-175
Manuscript under review for journal Geosci. Model Dev.
Discussion started: 4 August 2017

6.1 Detachment-limited comparison

With no sediment ($H = 0$ and $c_s = 0$) and $F_f = 1$ (all bedrock eroded becomes wash load and is not included in model calculations), all changes in bed elevation are driven by changes in bedrock elevation:

$$\frac{\partial \eta}{\partial t} = \frac{\partial R}{\partial t} \tag{36}$$

where

$$\frac{\partial R}{\partial t} = U - K_r q S^n - \omega_{cr}. \tag{37}$$

When $\omega_{cr} = 0$, Eq. (37) is the simple stream power model (Whipple and Tucker, 1999). At topographic steady state when $\frac{\partial R}{\partial t} = 0$ and $U = K_r q S^n$, the slope at every point in the channel is

$$S = \left(\frac{U}{K_r q} \right)^{1/n}. \tag{38}$$

Because we use a simple stream power formulation where $q = A^m$ for our test case, the slope-discharge relationship may be re-written to yield a slope-area relationship:

$$S = \left(\frac{U}{K_r A^m} \right)^{1/n}. \tag{39}$$

We test whether the SPACE component can replicate steady-state detachment-limited behavior by comparing slope-area relationships predicted by Eq. (39) with those calculated by the SPACE component. See table 1 for the parameter values used.

Figure 6 shows the results after the test model domain has achieved topographic steady state. The top panel of Fig. 6 shows the longitudinal profile of the longest drainage path in the model domain. As predicted by the theory described above, slope and drainage area trade off such that the outcome is a concave-up longitudinal profile with constant concavity. The lower panel of Fig. 6 compares the slope-area relationship predicted by Eq. (39) (gray dashed line) to the slope-area relationship in the steady-state model landscape (black dots). All core nodes from the model domain are shown, and every node obeys the predicted detachment-limited slope-area scaling. The slope of the slope-area power-law scaling relationship (Fig. 6) is the channel concavity, thus confirming that the channel concavity observed in the longitudinal profile is constant, and the SPACE component agrees with theoretical predictions for detachment-limited rivers at steady state.

6.2 Transport-limited comparison

When sediment thickness H is large relative to H_*, changes in bed elevation are driven entirely by changes in sediment bed elevation, which is set by the balance between sediment erosion, deposition, and rock uplift:

$$\frac{\partial \eta}{\partial t} = \frac{\partial H}{\partial t} = U + D_s - E_s. \tag{40}$$

At steady state, $\frac{\partial \eta}{\partial t} = 0$ and $E_s - D_s = U$. Substituting in the equations derived above for sediment erosion and deposition and assuming for simplicity that sediment porosity ϕ and the sediment erosion threshold ω_{cs} are negligible,

$$K_s q^m S^n - V \frac{Q_s}{Q} = U. \tag{41}$$

Geosci. Model Dev. Discuss., https://doi.org/10.5194/gmd-2017-175
Manuscript under review for journal Geosci. Model Dev.
Discussion started: 4 August 2017

Geoscientific Model Development Discussions
Open Access
EGU

Table 1. Parameter values for SPACE model test cases.

	Detachment Limited	Transport Limited	Mixed	Coupled
Number of rows (-)	20	20	20	50
Number of columns (-)	20	20	20	50
Node spacing (m)	100	100	100	100
Timestep (yr)	1	1	1	1
Run time (kyr)	100	100	200	300
Initial H (m)	0	100	0	0
U (m/yr)	0.0001	0.0001	0.0001	see text
K_r (yr^{-1})	0.001	0.0001	0.005	0.0001
K_s (yr^{-1})	0.01	0.01	0.01	0.0005
m (-)	0.5	0.5	0.5	0.5
n (-)	1.0	1.0	1.0	1.0
ω_{cr} (m/yr)	0	*	0	0
ω_{cs} (m/yr)	0	0	0	0
H_* (m)	1.0	1.0	1.0	1.0
ϕ (-)	0	0	0	0
F_f (-)	1	0	0	0
V (m/yr)	1.0	5.0	5.0	2.0

Not all parameters will influence the model outcome in all cases. For example, the value of V is irrelevant for the detachment-limited case when all eroded bedrock passes out of the model domain as permanently suspended fine sediment ($F_f = 1$).

Applying the steady-state mass conservation relationship $Q_s = UA$, recalling that $Q = rA$, and solving for S gives an expression for steady state channel slope:

$$S = \left[\frac{UV}{K_s q r} + \frac{U}{K_s q}\right]^{1/n}. \tag{42}$$

If $q = A^m$ as in our test case, the resulting slope-area relationship is then:

$$S = \left[\frac{UV}{K_s A^m r} + \frac{U}{K_s A^m}\right]^{1/n}. \tag{43}$$

Eq. (43) nicely distinguishes the contributions of sediment deposition (first term on the right side) and sediment entrainment (second term on the right side) to steady state channel slope. If effective settling velocity is negligible, erosion is only limited by the efficiency of sediment entrainment and Eq. (43) gives the detachment-limited steady state slope (though importantly the bed is still entirely composed of sediment). If entrainment and deposition of sediment are rapid enough that erosion is limited by transport capacity (i.e., the river has enough energy to erode more sediment but the water column is saturated), the system is transport-limited and the left hand term in Eq. (43) dominates in setting the steady state slope. Note the subtle difference

Geosci. Model Dev. Discuss., https://doi.org/10.5194/gmd-2017-175
Manuscript under review for journal Geosci. Model Dev.
Discussion started: 4 August 2017

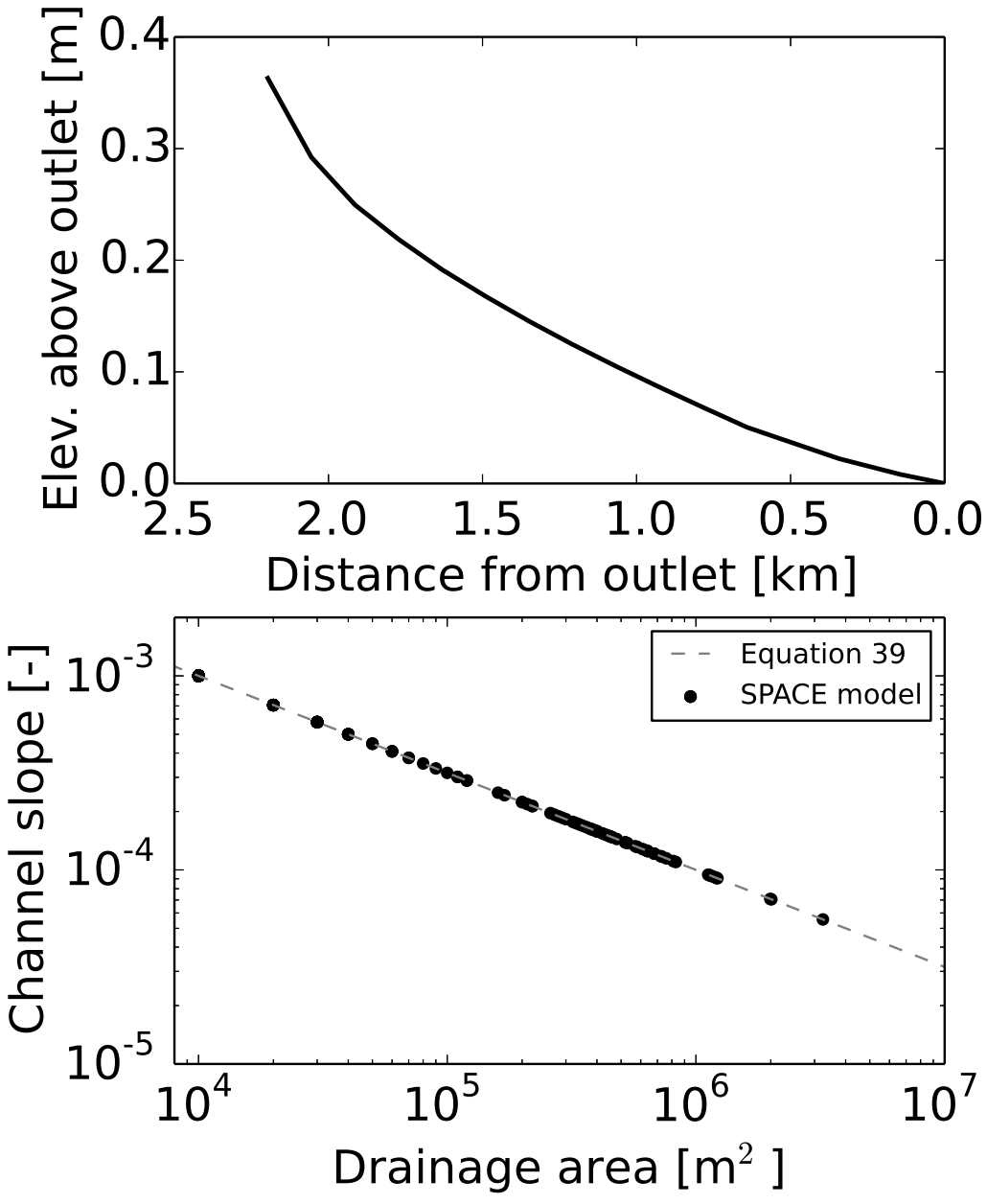

Figure 6. Top: longitudinal profile of the longest channel in the model domain under detachment-limited conditions, showing that the channel is in equilibrium with the imposed baselevel fall, and that the SPACE component yields concave-up longitudinal profiles at steady state. Bottom: comparison between the SPACE component and Eq. (39) (steady-state slope-area relationship under detachment-limited conditions). The numerical implementation of the SPACE component successfully replicates the predicted power-law slope-area relationship.

Geosci. Model Dev. Discuss., https://doi.org/10.5194/gmd-2017-175
Manuscript under review for journal Geosci. Model Dev.
Discussion started: 4 August 2017

between Eq. (43) and Eq. (18); when $H >> H_*$ and all surface lowering is accomplished by sediment entrainment, both terms on the right hand side of Eq. (43) reflect erosion of sediment (i.e., K_s is used in both). This occurs because when $H \gg H_*$, change in bedrock elevation over time is not zero as in true complete steady-state, but is equal to the uplift rate. Therefore, for topographic steady state to be achieved, both the transport and detachment terms of Eq. (43) must be accomplished through erosion of sediment. We compare the slope-area relationships predicted by Eq. (43) with those extracted from the SPACE model. In order to achieve conditions in which the transport term in Eq. (43) dominates, we set initial soil depth to 100 m everywhere on our test grid so that $H \gg H_*$. See Table 1 for all parameter values.

Figure 7 shows the results of the transport-limited model experiment. The top panel shows the longitudinal profile of the longest channel, and shows that the SPACE component produces concave-up longitudinal profiles at steady state under transport-limited conditions. The appearance of constant concavity in the longitudinal profile is verified by the constant slope in log-log space of the slope-area data shown in the middle panel of Fig. 7. The bottom panel compares the theoretical slope-area relationship (Eq. (43), gray dashed line in Fig. 2) with data from the model run (black dots). All core nodes from the model domain are included, and all agree well with the theoretical prediction. In addition to matching the analytical prediction for channel slope, the model also matches the expected steady-state sediment flux relationship, $Q_s = UA$ (Fig. 2, bottom panel). This indicates that the SPACE component is successfully matching expected transport-limited model behavior for both slope and sediment flux at steady state.

6.3 Mixed bedrock-alluvial comparison

One major advantage of SPACE over many existing fluvial erosion models is its ability to simultaneously compute the evolution of an alluvial layer and a bedrock surface. True steady state in the mixed bedrock-alluvial case occurs when the thickness of the alluvial layer H and the bedrock height R are both unchanging in time ($\frac{\partial H}{\partial t} = 0$ and $\frac{\partial R}{\partial t} = 0$). In such a scenario, $E_s = D_s$ and $U = E_r$. As described in Sect. 3.5, steady-state analytical solutions exist for channel slope, sediment thickness, and sediment flux (here again we use $q = A^m$ and keep $\phi = 0$ and $F_f = 0$):

$$S = \left[\frac{UV}{K_s A^m r} + \frac{U}{K_r A^m}\right]^{1/n}, \tag{44}$$

$$H = -H_* \ln\left[1 - \frac{V}{\frac{K_s r}{K_r} + V}\right], \tag{45}$$

and

$$Q_s = UA. \tag{46}$$

Running the SPACE component to complete steady state in a case where both sediment entrainment and bedrock erosion contribute to setting channel slope should therefore result in a concave-up channel profile with a sediment layer of constant thickness, and sediment flux equal to the product of the rock uplift rate and drainage area. We use the same tilted plane initial

Geosci. Model Dev. Discuss., https://doi.org/10.5194/gmd-2017-175
Manuscript under review for journal Geosci. Model Dev.
Discussion started: 4 August 2017

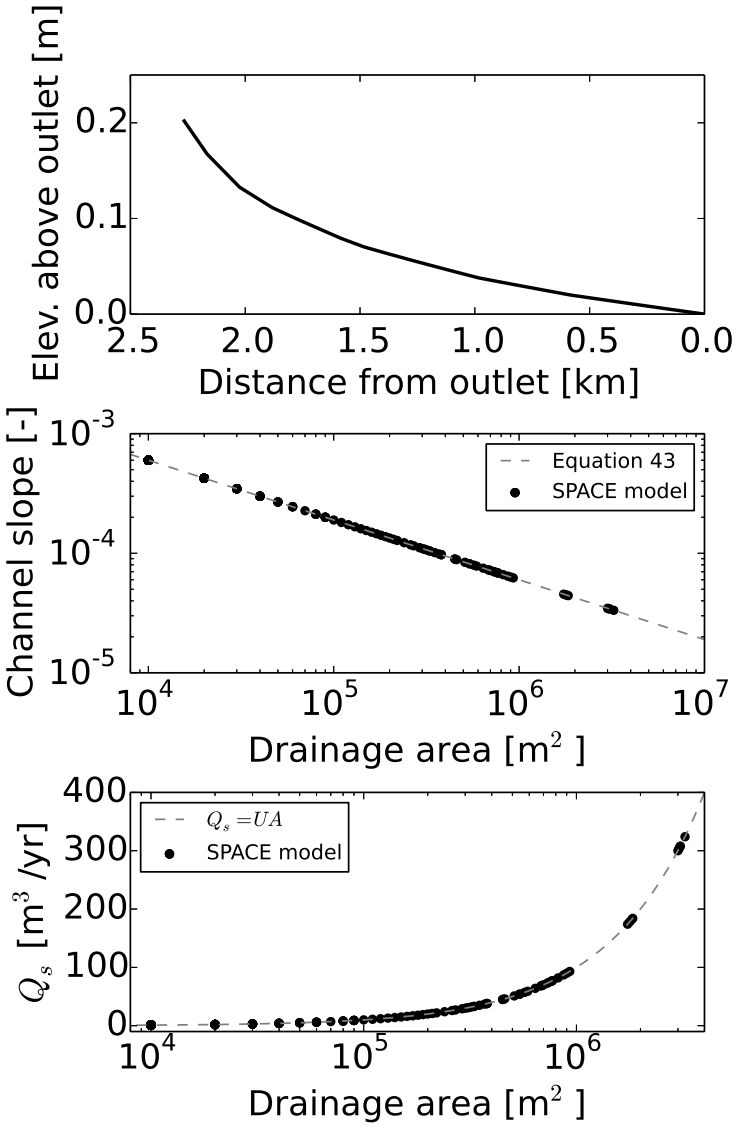

Figure 7. Top: longitudinal profile of the longest channel in the model domain under transport-limited conditions, showing that the channel is in equilibrium with the imposed baselevel fall, and that the SPACE component yields concave-up longitudinal profiles at steady state. Middle: comparison between the SPACE component and Eq. (43) (steady-state slope-area relationship under transport-limited conditions). The numerical implementation of the SPACE component successfully replicates the predicted power-law slope-area relationship. Bottom: Sediment flux Q_s as a function of drainage area. The model matches the predicted linear relationship $Q_s = UA$.

model domain as described in Sect. 6 to test whether the model can replicate the expected behavior in the bedrock-alluvial case. Matching the steady state analytical solutions requires both erosion of bedrock to generate the concave-up profile, and accumulation of sediment to a constant thickness over the landscape. We begin the numerical experiment with zero sediment

Geosci. Model Dev. Discuss., https://doi.org/10.5194/gmd-2017-175
Manuscript under review for journal Geosci. Model Dev.
Discussion started: 4 August 2017

thickness at all nodes. Table 1 shows all parameter values used. The driver script used for this model experiment is included in the code guide for this paper.

Figure 8 shows the evolution of the longitudinal bedrock profile and alluvial cover layer in the longest channel over several model timeslices. Beginning from a low-slope tilted plane, the channel incises bedrock and begins to build up a layer of alluvium on the channel bed. As model time progresses, the channel profile increases in concavity and the layer of alluvium thickens. Alluvial thickening progresses from downstream to upstream. By the final timeslice, the alluvial layer has reached its equilibrium value, the channel profile has equilibrated to the imposed uplift rate, and the bedrock surface, alluvium thickness, and topographic surface are all at steady state. Figure 9 shows the final channel profile (top panel) when the topographic surface, sediment thickness, and bedrock height are all at steady state. The topographic surface (top of the sediment layer) is everywhere parallel to the bedrock surface, and the bed sediment layer is 1.25 m thick at every point along the channel profile. Given $V = 5$ m/s, $K_s = 0.01$ yr^{-1}, and $K_r = 0.005$ yr^{-1}, as used in the model, the steady state sediment thickness of $H = 1.25$ m calculated by the model matches the analytical prediction of Eq. (20). The middle panel compares the theoretical prediction for slope-area scaling given by Eq. (44) (gray dashed line) with the model results (black dots). As in the detachment-limited and transport-limited cases, the model matches the analytical prediction. The bottom panel of Fig. 9 compares the theoretical steady state relationship between drainage area and sediment flux ($Q_s = UA$) with modeled sediment flux, and shows that the model shows the predicted linear increase in Q_s with drainage area. The ability of the SPACE component to treat both the detachment-limited and transport-limited end members of fluvial systems as well as the mixed bedrock-alluvial case confirms that the model equations are being solved correctly, and importantly that our use of stabilizing, local analytical solutions does not compromise the ability of the model to replicate expected behavior. The results of the three tests presented above indicate that the SPACE component is useful for modeling river evolution across a wide variety of natural settings. Below, we show how the SPACE component may be efficiently coupled with other surface processes models in the Landlab modeling framework to provide insight into landscape evolution.

7 Application to landscape evolution modeling: Coupling SPACE with hillslope diffusion to model topographic growth and decay

One frequent application of landscape evolution modeling is the exploration of landscape response to tectonic perturbations. Understanding the growth and decay of topography has significant implications for interpretation of the stratigraphic record, which is composed of sediment that is detached and transported from upland landscapes. In this section we show how the SPACE component can be coupled with a hillslope diffusion model in the Landlab modeling toolkit to simulate landscape response to changing rock uplift rates. In addition to computing topographic change that incorporates both sediment and bedrock surface evolution, we show the capability of the SPACE component to provide information about sediment fluxes delivered from the model catchment over time.

Geosci. Model Dev. Discuss., https://doi.org/10.5194/gmd-2017-175
Manuscript under review for journal Geosci. Model Dev.
Discussion started: 4 August 2017

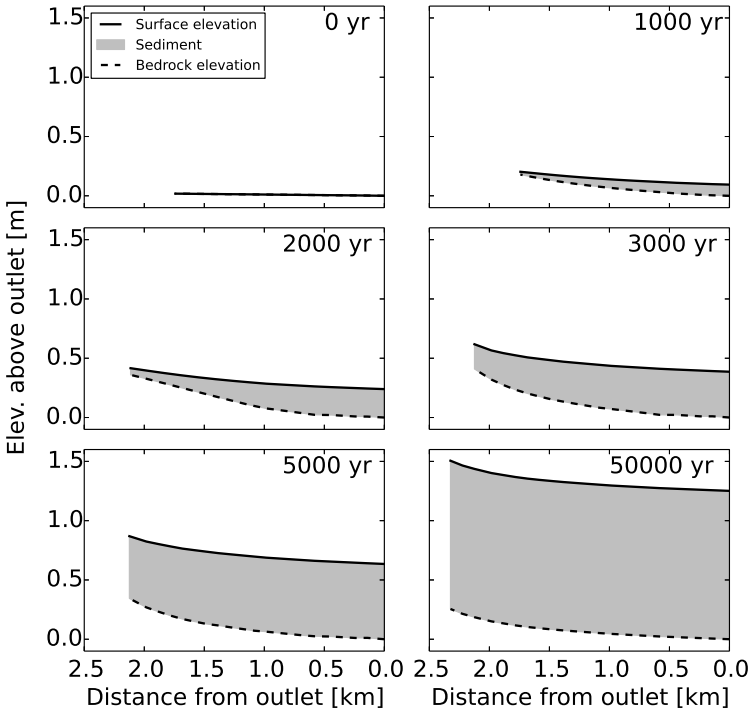

Figure 8. Time series of longitudinal profile evolution for the longest channel in the test model domain as the domain is uplifted relative to baselevel. Profile distance lengthens over time as the original tilted ramp is incised; horizontal scale on all plots is the same. Initially (0 yr), the channel topographic surface is effectively flat with zero sediment thickness. By 1000 yr, a slightly concave-up bedrock profile has developed, with a thin, downstream-thickening layer of bed sediment resulting in a surface profile that is less concave-up than the bedrock profile. Over the following three timeslices, continued rock uplift relative to baselevel causes increased concavity in the bedrock profile, as well as continued thickening of the sediment layer. The sediment layer thickness in a downstream to upstream progression. By 50,000 yr, the sediment layer has uniform thickness, resulting in a surface profile of equal concavity to the bedrock profile, and the alluvial layer thickness, topographic surface elevation, and bedrock surface elevation are all equilibrated to the imposed rock uplift rate and are therefore unchanging in time. Vertical exaggeration $\approx 1100\times$.

7.1 Model setup

We use a Landlab raster model grid composed of 2500 nodes (50 x 50 grid). We use a node spacing ($\mathrm{d}x$) of 100 m, resulting in a 25 km^2 area grid. As with the model verification experiments described above, we close all model domain boundaries except for a single open outlet in the lower-left (southwest) corner. The use of a single outlet means that the entire model domain will be a single watershed draining to the outlet, and the sediment flux leaving the outlet is the integrated sediment flux from the entire basin. Our landscape initial condition is a plane tilted slightly (initial regional slope of $\approx 1.4 \times 10^{-5}$) towards the basin outlet. The tilted plane has initial, random sub-millimeter scale surface roughness to initiate the formation of drainage pathways.

Geosci. Model Dev. Discuss., https://doi.org/10.5194/gmd-2017-175
Manuscript under review for journal Geosci. Model Dev.
Discussion started: 4 August 2017

Geoscientific Model Development Discussions

For simplicity we use the simple stream power form of the SPACE model ($m = 0.5$, $n = 1$, $q = A^m$) and keep $\phi = 0$ and $F_f = 0$. We do not incorporate sediment entrainment and bedrock erosion thresholds. See Table 1 for all SPACE parameter values used in this example. We couple this parameterization of the SPACE component with Landlab's linear diffusion component, which computes the topographic-gradient-driven movement of mass at every node by the equation

$$\frac{\partial \eta}{\partial t} = \kappa \frac{\partial^2 \eta}{\partial x^2} \tag{47}$$

where κ is a diffusivity in units of [L^2/T] (we use $\kappa = 0.005$ m^2/yr). Programmatically, we incorporate Eq. (47) simply by running Landlab's linear diffusion component immediately after running the SPACE component in each model timestep. One simplification made by simple linear diffusion models is that the entire landscape is made of the same material (i.e., no distinction between rock and soil). To realistically couple linear diffusion with our fluvial erosion model that explicitly separates the dynamics of sediment and bedrock, we assume that any material diffused from one model node onto another is sediment. Such an assumption is realistic given the purpose and limitations of the linear diffusion model, which has been shown to apply primarily to soil-mantled hillslopes.

We ran our coupled model with a 1 year timestep for 300,000 years. Because our goal is to use SPACE and linear diffusion to explore topographic growth and decay, we used a rock uplift rate U relative to baselevel that was unsteady in time. We simulated a "pulse" of rapid rock uplift preceded and followed by periods of slower rock uplift. U was set to 0.0001 m/yr for the first 100 kyr, increased to 0.0005 m/yr for the second 100 kyr, and returned to 0.0001 m/yr for the final 100 kyr. Two variables of broad interest that generally vary in response to changing rock uplift rates are topographic relief and total sediment flux out of the model catchment. We predict under such a scenario that topographic relief and sediment flux will increase as surface erosion responds to rock uplift for the first 200 kyr, and that relief and sediment flux will reach their maximum when the rock uplift rate is at its highest value. We then expect decays in relief and sediment flux as the high points in the landscape erode and topographic gradients shrink in response to a return to the lower rock uplift rate. We recorded the topographic elevation at all model nodes, along with relief and sediment flux from the domain, at 1 kyr intervals.

7.2 Results of coupled model experiment

Figure 10 shows several timeslices of model topography showing the response to imposed rock uplift, and Fig. 11 shows sediment depth over the model domain at the same timeslices. Over the first 100 kyr, bedrock incision into the initially non-alluviated domain dominates adjustment to rock uplift. However, because the rock uplift rate is low and topographic gradients are being lowered by fluvial erosion and hillslope diffusion, the landscape has < 10 m of relief after 100 kyr. Sediment is first produced on the hillslopes (the products of diffusion are considered to be sediment) but not stored in the channels for the first 50 kyr as the channels incise into bedrock to accommodate the onset of rock uplift. By 100 kyr, the landscape is nearly equilibrated to the rock uplift rate, and alluviation has occurred in the channels as sediment thickness approaches its equilibrium value everywhere. Between 100 and 200 kyr, during which the rock uplift rate is five times its initial value, the network progressively develops higher and higher relief (up to ≈ 50 m) until the rock uplift rate is reduced again at 200 kyr. During this period, the channels initially strip their alluvial cover and incise bedrock to match the increased rock uplift

Geosci. Model Dev. Discuss., https://doi.org/10.5194/gmd-2017-175
Manuscript under review for journal Geosci. Model Dev.
Discussion started: 4 August 2017

rate. However, as in the first 100 kyr, as the landscape begins to equilibrate to the new rock uplift rate by 200 kyr, alluvium thickness again increases towards its equilibrium condition. Once the rock uplift rate is reduced, diffusion of material from the hillslopes into the channels results in sediment mantling of the channels and significant reduction of the rate of bedrock incision. By 300 kyr, the lowering of high points by diffusion, together with the inability of low-gradient, sediment-mantled rivers to effectively incise bedrock, has resulted in reductions in landscape relief such that the landscape at 300 kyr nearly mirror the 100 kyr timeslice (≈ 10 m of relief). At this point, the reduction in topographic gradients has reduced sediment delivery to the channels, which begin to strip their alluvial cover down to its equilibrium thickness.

The patterns observed in Fig. 10 and Fig. 11 are quantified in Fig. 12. Relief and sediment flux out of the model domain increase initially as the landscape is adjusting, through bedrock incision, from its initial condition to become equilibrated with the imposed rock uplift rate. The rates of increase in both relief and sediment flux increase substantially as the rock uplift rate quintuples at 100 kyr, and while neither reaches its equilibrium value (i.e., steady in time), both relief and sediment flux begin to asymptote towards those equilibrium values. At 200 kyr when the rock uplift rate is reduced to its initial value, diffusion rapidly reduces topographic gradients and alluviates channels, and channels become less erosive. Thus both relief and sediment flux decline over the final 100 kyr of the experiment, again approaching, but not fully reaching, their steady state values. The simple experiment performed here shows that the SPACE component may be easily coupled with other models of earth surface processes in Landlab to explore any number of questions relating to landscape evolution. While 1-D models of river longitudinal profile evolution have proliferated widely over the past decades, 2-D models that explicitly incorporate sediment morphodynamics and bedrock erosion simultaneously are rare, and those that are easily coupled with other models are even rarer. The SPACE algorithm and component fill an important gap in the quantitative geomorphologists's toolkit, and it is our hope that future users will apply it, potentially in conjunction with other Landlab components, to solve diverse geomorphological problems.

8 Limitations of the SPACE model

The SPACE model is intended to provide a simple, extensible, easy-to-use tool to expand the set of questions that can be addressed with numerical models of river channel evolution. We have consolidated recent advances in the treatment of sediment erosion and deposition (Davy and Lague, 2009) as well as simultaneous evolution of sediment and bedrock layers (Lague, 2010; Zhang et al., 2015) into a single model that has the additional advantages of being 2-D, easily accessible, and easily coupled to other surface processes models in the Landlab modeling toolkit. As such, our model encompasses some of the same limitations as the previous work from which it is derived, including a lack of dynamic channel width and a lack of treatment of the tools effect.

To allow efficient solution of the SPACE model over large model grids and timescales, we do not incorporate the hydrodynamic calculations (i.e., explicit computation of stresses on the bed and banks) required to allow channel width to evolve freely (e.g., Stark, 2006; Wobus et al., 2006; Davy and Lague, 2009; Lague, 2010; Coulthard et al., 2013). Instead, we employ a common parameterization for channel width as a function of drainage area or discharge. In the examples in this paper we

Geosci. Model Dev. Discuss., https://doi.org/10.5194/gmd-2017-175
Manuscript under review for journal Geosci. Model Dev.
Discussion started: 4 August 2017

Geoscientific Model Development Discussions

used a width scaling of $w = Q^{0.5}$, which results in $q = Q^{0.5}$ or $q = A^{0.5}$ if drainage area is used as a surrogate for discharge. The width scaling exponent m, which we held equal to 0.5 in the examples discussed here, is a user-defined parameter. The use of an empirical width scaling means that 1) any given point along the channel occupies a single grid cell regardless of whether width is less than, equal to, or greater than grid cell size, and 2) SPACE does not capture temporal channel width variations in response to rock uplift, sediment flux, and discharge changes. In some cases, channel width may respond more significantly than channel slope to such forcings (e.g., Amos and Burbank, 2007; Turowski et al, 2009). While our use of a downstream width relationship enables us to test the SPACE model against known analytical solutions and eliminates the need for hydrodynamic calculations, the future addition of dynamic width would allow exploration of the relative importance of slope and width adjustment.

The SPACE model as presented here follows previous models in treating reduction of bedrock erosion by sediment cover (e.g., Beaumont et al., 1992; Lague, 2010; Shobe et al., 2016), but does not include the enhancement of bedrock erosion by the presence of mobile bedload tools (e.g., Sklar and Dietrich, 2004; Gasparini et al., 2006; Turowski et al., 2007; Zhang et al., 2015). Such a simplification keeps expected model behavior conceptually simple and allows comparison of model results to known analytical solutions for the purposes of model validation. However, there is substantial field evidence indicating that mobilized bedload can be an important erosive agent, especially where bedrock is too widely jointed to permit plucking of bedrock blocks (Hancock et al., 1998; Cook et al., 2013; Beer et al., 2016). The major effect of excluding this effect from the SPACE model is that bedrock erosion will be underpredicted at low to moderate sediment fluxes, where there is enough bedload to frequently abrade the bed, but not enough to form a deep layer of alluvial cover. Adding the tools effect to the SPACE model could be accomplished by changing the form of the bedrock erosion function to mimic the parabolic (Sklar and Dietrich, 2004), almost-parabolic (Gasparini et al., 2006), or similar (Turowski et al., 2007) dependence of erosion efficiency on Q_s or H/H_*.

9 Conclusions

We have developed and presented a new model for sediment transport and river incision into bedrock. The SPACE model is a significant advance over standard sediment-flux-dependent river incision models because it explicitly treats sediment morphodynamics rather than relying on a parameterized relationship between sediment flux and transport capacity. SPACE is based on the erosion-deposition framework outlined by Davy and Lague (2009), and is able to transition between detachment-limited, transport-limited, and mixed cases. Further, in contrast to the erosion-deposition model, our model simultaneously evolves a sediment layer and the underlying bedrock surface. In this regard, our model is similar to those proposed by Lague (2010) and Zhang et al. (2015). We make some simplifications relative to those models, excluding dynamic width variation (e.g., Lague, 2010) and "tools" effects (e.g., Zhang et al., 2015) from our modeling framework.

We developed steady-state analytical solutions for channel slope, sediment thickness, and sediment flux in Sect. 3.5 based on the model governing equations. We then showed three experiments in section 5 demonstrating that the numerical implemen-

tation of SPACE, which uses local analytical solutions for stable calculation of sediment flux and sediment thickness, matches the analytical predictions at steady state in the detachment-limited, transport-limited, and mixed bedrock-alluvial cases.

The foremost advantage of SPACE over other similar models is its ease of use for modeling landscape evolution in two dimensions. The SPACE 1.0 component is implemented in 2-D as part of the freely available Landlab modeling toolkit, and may be readily coupled to other models of earth surface processes. We showed in an example application how the SPACE component may be coupled to a linear diffusion hillslope evolution model to investigate the growth and decay of topography in response to temporally variable rock uplift. The unique ability of SPACE to separately evolve bedrock topography and sediment thickness makes it well-suited to a suite of possible applications that are out of reach for simpler, bedrock-only or sediment-flux-dependent river incision models. For example, the SPACE component would be effective for modeling the depositional filling of flexural depressions, downthrown fault blocks, and landslide-dammed rivers. In situations where temporal variability in sediment flux is a variable of interest, the ability of SPACE to store sediment in the form of an alluvial layer could yield more realistic results than simple detachment- or transport-limited models. Finally, the SPACE modeling framework is flexible in that the stream-power based entrainment and erosion equations (Eq. (7 and 8)) may be replaced with other formulations better tailored to individual model applications.

The SPACE 1.0 component enables 2-D calculation of sediment transport, bedrock erosion, and landscape evolution within the Landlab modeling toolkit. The model's ability to simultaneously transport sediment and erode bedrock opens up a wide variety of potential applications beyond the limits of simpler models. SPACE may be easily coupled to other models in Landlab to address novel questions in geomorphology.

10 Code availability

The SPACE 1.0 Landlab component as well as all other Landlab components used in this paper are part of Landlab version 1.0.2. Source code for the Landlab project is housed on GitHub: http://github.com/landlab/landlab. Documentation, installation instructions, and software dependencies for the entire Landlab project can be found at http://landlab.github.io/. A detailed user manual with an accompanying Jupyter notebook and a driver script for the mixed bedrock-alluvial example illustrated in this paper can be found at https://github.com/cmshobe/pub_shobe_etal_GMD (Shobe, 2017, GitHub Repository). The Landlab project is tested on recent-generation Mac, Linux, and Windows platforms using Python versions 2.7, 3.4, and 3.5. The Landlab modeling framework is distributed under a MIT open-source license.

Author contributions. GET developed the algorithm. CMS implemented the algorithm, wrote the Landlab component with help from KRB, verified and evaluated the model solutions, and wrote the paper with contributions from GET and KRB.

Competing interests. The authors declare that they have no conflicts of interest.

Geosci. Model Dev. Discuss., https://doi.org/10.5194/gmd-2017-175
Manuscript under review for journal Geosci. Model Dev.
Discussion started: 4 August 2017

Acknowledgements. This work was supported by National Science Foundation grants ACI-1147454 (PI: Gregory E. Tucker) and ACI-1450409 (PI: Gregory E. Tucker), and a National Defense Science and Engineering Graduate fellowship to Charles M. Shobe. Thanks to Jordan Adams, Alexandra Carriere, Rachel Glade, Harrison Gray, Aaron Hurst, Kelly Kochanski, Caroline Le Bouteiller, and Matt Rossi for helpful discussions.

References

Adams, J. M., Gasparini, N. M., Hobley, D. E. J., Tucker, G. E., Hutton, W. E. H., Nudurupati, S. S., and Istanbulluoglu, E.: The Landlab v1.0 OverlandFlow component: a Python tool for computing shallow-water flow across watersheds, Geosci. Mod. Dev., 10, 1645-1663, doi:10.5194/gmd-10-1645-2017, 2017.

Amos, C. B., and Burbank, D. W.: Channel width response to differential uplift, J. Geophys. Res., 112, F02010, doi:10.1029/2006JF000672, 2007.

Armitage, J. J., Duller, R. A., Whittaker, A. C., and Allen, P. A.: Transformation of tectonic and climatic signals from source to sedimentary archive, Nature Geoscience, 4, 231-235, doi:10.1038/NGEO1087, 2011.

Beaumont, C., Fullsack, P., and Hamilton, J.: Erosional control of active compressional orogens, in Thrust Tectonics, edited by K. R. McClay, 1-18, 1992.

Beer, A. R., Turowski, J. M., and Kirchner, J. W.: Spatial patterns of erosion in a bedrock gorge, J. Geophys. Res. Earth Surf., 122, doi:10.1002/2016JF003850.

Braun, J. and Sambridge, M.: Modeling landscape evolution on geological time scales: A new method based on irregular spatial discretization, Basin Research, 9, 27-52, 1997.

Braun, J. and Willett, S. D.: A very efficient, O(n), implicit and parallel method to solve the stream power equation governing fluvial incision and landscape evolution, Geomorphology, 180-181, 170-179, doi:10.1016/j.geomorph.2012.10.008, 2013.

Carretier, S., Martinod, P., Reich, M., and Godderis, Y.: Modelling sediment clasts transport during landscape evolution, Earth Surf. Dynam., 4, 237-251, doi:10.5194/esurf-4-237-2016, 2016.

Clark, M. P. and Kavetski, D.: Ancient numerical daemons of conceptual hydrological modeling: 1. Fidelity and efficiency of time stepping schemes, Water Resour. Res., 46(10), W10510, doi:10.1029/2009WR008894, 2010.

Cook, K. L., Turowski, J. M., and Hovius, N.: A demonstration of the importance of bedload transport for fluvial bedrock erosion and knickpoint propagation, Earth Surf. Proc. Land., 38, 683-695, doi:10.1002/esp.3313, 2013.

Coulthard, T. J., Macklin, M. G., and Kirkby, M. J.: A cellular model of Holocene upland river basin and alluvial fan evolution, Earth Surf. Proc. Land., 27, 269-288, doi:10.1002/esp.318, 2002.

Coulthard, T. J., Neal, J. C., Bates, P. D., Ramirez, J., de Almeida, G. A. M., and Hancock, G. R.: Integrating the LISFLOOD-FP 2D hydrodynamic model with the CAESAR model: implications for modelling landscape evolution, Earth Surf. Proc. Land., 38(15), 1897-1906, doi:10.1002/esp.3478, 2013.

Davy, P. and Lague, D.: Fluvial erosion/transport equation of landscape evolution models revisited, J. Geophys. Res.-Earth, 114, F03007, doi:10.1029/2008JF001146, 2009.

DiBiase, R. A. and Whipple, K. X.: The influence of erosion thresholds and runoff variability on the relationships among topography, climate, and erosion rate, J. Geophys. Res., 116, F04036, doi:10.1029/2011JF002095, 2011.

Ferguson, R. I., Sharma, B. P., Hardy, R. J., Hodge, R. A., and Warburton, J.: Flow resistance and hydraulic geometry in contrasting reaches of a bedrock channel, Water Resour. Res., 53, 2278-2293, doi:10.1002/2016WR020233, 2017.

Gasparini, N. M., Bras, R. L., and Whipple, K. X.: Numerical modeling of non-steady-state river profile evolution using a sediment-flux-dependent incision model, Geol. Soc. Am. Spec. Pap., 398, 127-141, 2006.

Gasparini, N. M., Whipple, K. X., and Bras, R. L.: Predictions of steady state and transient landscape morphology using sediment-flux-dependent river incision models, J. Geophys. Res., 112, F03S09, doi:10.1029/2006JF000567, 2007.

Graf, W. L., Wohl, E., Sinha, T., and Sabo, J. L.: Sedimentation and sustainability of western American reservoirs, Water Resour. Res., 46, W12535, doi:10.1029/2009WR008836, 2010.

Hancock, G. S., Anderson, R. S., and Whipple, K. X.: Beyond power: Bedrock river process and form, in Rivers Over Rock: Fluvial Processes in Bedrock Channels, Geophys. Monger. Ser., vol. 107, edited by K. J. Tinkler and E. E. Wohl, 35-60, 1998.

Hancock, G. S., Small, E. E., and Wobus, C. W.: Modeling the effects of weathering on bedrock-floored channel geometry, J. Geophys. Res., 116, F03018, doi:10.1029/2010JF001908, 2011.

Hilton, R. G.: Climate regulates the erosional carbon export from the terrestrial biosphere, Geomorphology, 277, 118-132, doi:10.1016/j.geomorph.2016.03.028, 2017.

Hobley, D. E. J., Sinclar, H. D., Mudd, S. M., and Cowie, P. A.: Field calibration of sediment flux dependent river incision, J. Geophys. Res., 116, F04017, doi:10.1029/2010JF001935, 2011.

Hobley, D. E. J., Adams, J. M., Nudurupati, S. S., Hutton, E. W. H., Gasparini, N. M., Istanbulluoglu, E., and Tucker, G. E.: Creative computing with Landlab: an open-source toolkit for building, coupling, and exploring two-dimensional numerical models of Earth-surface dynamics, Earth Surf. Dynam., 5, 21-46, doi:10.5194/esurf-5-21-2017, 2017.

Hodge, R. A., Hoey, T. B., and Sklar, L. S.: Bed load transport in bedrock rivers: The role of sediment cover in grain entrainment, translation, and deposition, J. Geophys. Res., 116, F04028, doi:10.1029/2011JF002032, 2011.

Hodge, R. A. and Hoey, T. B.: Upscaling from grain-scale processes to alluviation in bedrock channels using a cellular automaton model, J. Geophys. Res., 117, F01017, doi:10.1029/2011JF002145, 2012.

Hodge, R. A.: Sediment processes in bedrock-alluvial rivers: Research since 2010 and modeling the impact of fluctuating sediment supply on sediment cover, in: Gravel-bed Rivers: Gravel Bed Rivers and Disasters, 2017.

Howard, A. D.: A detachment-limited model of drainage-basin evolution, Water Resour. Res., 30, 2261-2285, doi:10.1029/94wr00757, 1994.

Johnson, J. P. L., Whipple, K. X., Sklar, L. S., and Hanks, T. C.: Transport slopes, sediment cover, and bedrock channel incision in the Henry Mountains, Utah, J. Geophys. Res., 114, F02014, doi:10.1029/2007JF000862, 2009.

Johnson, J. P. L.: A surface roughness model for predicting alluvial cover and bed load transport rate in bedrock channels, J. Geophys. Res. Earth Surf., 119, 2147-2173, doi:10.1002/2013JF003000, 2014.

Johnson, J. P. L.: Gravel threshold of motion: A state function of sediment transport disequilibrium? Earth Surf. Dynam., 4, 685-703, doi:10.5194/esurf-4-685-2016, 2016.

Johnson, K. N. and Finnegan, N. J.: A lithologic control on active meandering in bedrock channels, Geol. Soc. Am. Bull., 127, 11/12, 1766-1776, doi:10.1130/B31184.1, 2015.

Kavetski, D. and Clark, M. P.: Ancient numerical daemons of conceptual hydrological modeling: 2. Impact of time stepping schemes on model analysis and prediction, Water Resour. Res., 46(10), W10511, doi:10.1029/2009WR008896, 2010.

Lague, D., Crave, A., and Davy, P.: Laboratory experiments simulating the geomorphic response to tectonic uplift, J. Geophys. Res., 108, B1, 2008, doi:10.1029/2002JB001785, 2003

Lague, D., Hovius, N., and Davy, P.: Discharge, discharge variability, and the bedrock channel profile, J. Geophys. Res., 110, F04006, doi:10.1029/2004JF000259, 2005.

Lague, D.: Reduction of long-term bedrock incision efficiency by short-term alluvial cover intermittency, J. Geophys. Res., 115, F02011, doi:10.1029/2008JF001210, 2010.

Lajeunesse, E., Devauchelle, O., Lachaussée, F., and Claudin, P.: Bedload transport in laboratory rivers: The erosion-deposition model, in: Gravel-bed Rivers: Gravel Bed Rivers and Disasters, 2017.

Lamb, M. P., Dietrich, W. E., and Sklar, L. S.: A model for fluvial bedrock incision by impacting suspended and bed load sediment, J. Geophys. Res., 113, F03025, doi:10.1029/2007JF000915, 2008.

Leopold, L. B. and Maddock, T.: The hydraulic geometry of stream channels and some physiographic implications, U.S. Geol. Sure. Prof. Pap., 252, 1953.

Murphy, B. P., Johnson, J. P. L., Gasparini, N. M., and Sklar, L. S.: Chemical weathering as a mechanism for the climatic control of bedrock river incision, Nature, 532, doi:10.1038/nature17449, 2016.

Paola, C. and Voller, V. R.: A generalized Exner equation for sediment mass balance, J. Geophys. Res., 110, F04014, doi:10.1029/2004JF000274, 2005.

Shobe, C. M., Tucker, G. E., and Anderson, R. S.: Hillslope-derived blocks retard river incision, Geophys. Res. Lett., 43, 10, 5070-5078, doi:10.1002/2016GL069262, 2016.

Shobe, C. M.: GitHub Repository: SPACE example drivers and documentation, doi:10.6084m9.figshare.5193478.v1, 2017.

Shobe, C. M., Hancock, G. S., Eppes, M. C., and Small, E. E.: Field evidence for the influence of weathering on rock erodibility and channel form in bedrock rivers, Earth Surf. Proc. Land., doi:10.1002/esp.4163, 2017.

Sklar, L. S. and Dietrich, W. E.: River longitudinal profiles and bedrock incision models: Stream power and the influence of sediment supply, in Rivers Over Rock: Fluvial Processes in Bedrock Channels, Geophys. Monger. Ser., vol. 107, edited by K. J. Tinkler and E. E. Wohl, 237-260, 1998.

Sklar, L. S. and Dietrich, W. E.: Sediment and rock strength controls on river incision into bedrock, Geology, 29, 12, 1087-1090, 2001.

Sklar, L. S. and Dietrich, W. E.: A mechanistic model for river incision into bedrock by saltating bed load, Water Resour. Res., 40, W06301, 2004.

Small, E. E., Blom, T., Hancock, G. S., Hynek, B. M., and Wobus, C. W.: Variability of rock erodibility in bedrock-floored stream channels based on abrasion mill experiments, J. Geophys. Res. Earth Surf., 120, 1455-1469, doi:10.1002/2015JF003506, 2015.

Snyder, N. P., Whipple, K. X., Tucker, G. E., and Merritts, D. J.: Importance of a stochastic distribution of floods and erosion thresholds in the bedrock river incision problem, J. Geophys. Res., 108, B2, 2117, doi:10.1029/2001JB001655, 2003.

Stark, C. P.: A self-regulating model of bedrock river channel geometry, Geophys. Res. Let., 33, L04402, doi:10.1029/2005GL023193, 2006.

Stock, J. D. and Montgomery, D. R.: Geologic constraints on bedrock river incision using the stream power law, J. Geophys. Res., 104, B3, 4983-4993, 1999.

Tomkin, J. H., Brandon, M. T., Pazzaglia, F. J., Barbour, J. R., Willett, S. D.: Quantitative testing of bedrock incision models for the Clearwater River, NW Washington State, J. Geophys. Res., 108, B6, 2308, doi:10.1029/2001JB000862, 2003.

Tucker, G. E.: Drainage basin sensitivity to tectonic and climatic forcing: Implications of a stochastic model for the role of entrainment and erosion thresholds, Earth Surf. Proc. Land., 29, 185?205, 2004.

Tucker, G. E., Lancaster, S. T., Gasparini, N. M., and Bras, R. L.: The Channel-Hillslope Integrated Landscape Development (CHILD) model, in Landscape Erosion and Evolution Modeling, edited by R. S. Harmon and W. W. Doe III, 349-388, 2001.

Tucker, G. E., Hobley, D. E. J., Hutton, E., Gasparini, N. M., Istanbulluoglu, E., Adams, J. M., and Nudurupati, S. S.: CellLab-CTS 2015: continuous-time stochastic cellular automa- ton modeling using Landlab, Geosci. Model Dev., 9, 823?839, doi:10.5194/gmd-9-823-2016, 2016.

Turowski, J. M., Lague, D., and Hovius, N.: Cover effect in bedrock abrasion: A new derivation and its implications for the modeling of bedrock channel morphology, J. Geophys. Res., 112, F04006, doi:10.1029/2006JF000697, 2007.

Turowski, J. M., Lague, D., and Hovius, N.: Response of bedrock channel width to tectonic forcing: Insights from a numerical model, theoretical considerations, and comparison with field data, J. Geophys. Res., 114, F03016, doi:10.1029/2008JF001133, 2009.

Valla, P. G., van der Beek, P. A., and Lague, D.: Fluvial incision into bedrock: Insights from morphometric analysis and numerical modeling of gorges incising glacial hanging valleys (Western Alps, France), J. Geophys. Res. Earth Surf., 115, F2, doi:10.1029/2008JF001079, 2010.

van der Beek, P. and Bishop, P.: Cenozoic river profile development in the Upper Lachlan catchment (SE Australia) as a test of quantitative fluvial incision models, J. Geophys. Res., 108, B6, 2309, doi:10.1029/2002JB002125, 2003.

Whipple, K. X.: Bedrock rivers and the geomorphology of active orogens, Annu. Rev. Earth Planet. Sci., 32, 151-185, doi:10.1146/annurev.earth.32.101802.120356, 2004.

Whipple, K. X. and Tucker, G. E.: Dynamics of the stream-power river incision model: Implications for height limits of mountain ranges, landscape response timescales, and research needs, J. Geophys. Res., 104(B8), 17,661?17,674, doi:10.1029/1999JB900120, 1999.

Whipple, K. X., Hancock, G. S., and Anderson, R. S.: River incision into bedrock: Mechanics and relative efficacy of plucking, abrasion, and cavitation, Geol. Soc. Am. Bull., 112(3), 490?503, 2000.

Whipple, K. X. and Tucker, G. E.: Implications of sediment-flux-dependent river incision models for landscape evolution, J. Geophys. Res., 107, B2, 2039, doi:10.1029/2000JB000044, 2002.

Willgoose, G. R., Bras, R. L., and Rodriguez-Iturbe, I.: A physically based coupled network growth and hillslope evolution model: 1, Theory, Water Resour. Res., 27, 1671-1684, 1991.

Wobus, C. W., Tucker, G. E., and Anderson, R. S.: Self-formed bedrock channels, Geophys. Res. Let., 33, L18408, doi:10.1029/2006GL027182, 2006.

Zhang, L., Parker, G., Stark, C. P., Inoue, T., Viparelli, E., Fu, X., and Izumi, N.: Macro-roughness model of bedrock-alluvial river morphodynamics, Earth Surf. Dynam., 3, 113-138, 2015.

Geosci. Model Dev. Discuss., https://doi.org/10.5194/gmd-2017-175
Manuscript under review for journal Geosci. Model Dev.
Discussion started: 4 August 2017

Geoscientific Model Development Discussions

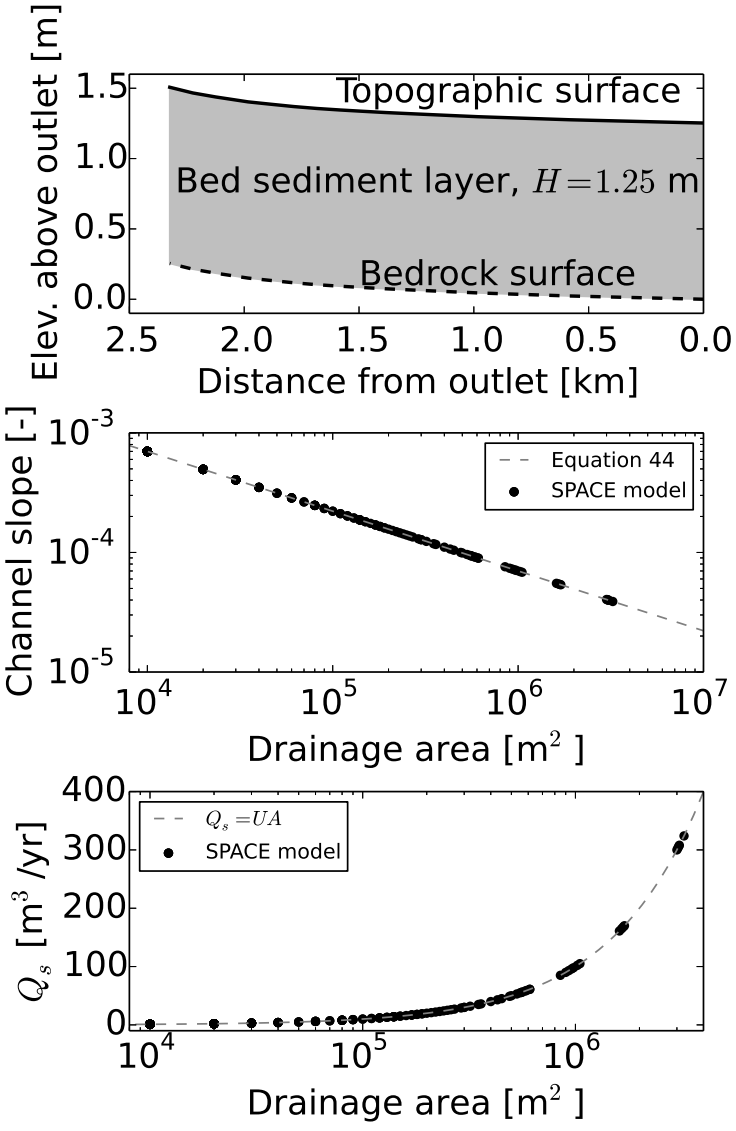

Figure 9. Top: longitudinal profile of the longest channel in the model domain after 200 kyr of model time during which the channel has evolved from an initial condition of zero sediment thickness to a constant, steady sediment thickness. Both the topographic surface (top of the sediment layer) and the bedrock surface are in equilibrium with the imposed baselevel fall, showing that the SPACE component yields parallel, concave-up longitudinal profiles in sediment and bedrock at steady state. The sediment thickness H matches the predicted sediment thickness for the parameters used in the model run. Middle: comparison between the SPACE component and Eq. (44) (steady-state slope-area relationship under bedrock-alluvial conditions). The numerical implementation of the SPACE component successfully replicates the predicted power-law slope-area relationship. Bottom: Sediment flux Q_s as a function of drainage area. The model matches the predicted linear relationship $Q_s = UA$.

Geosci. Model Dev. Discuss., https://doi.org/10.5194/gmd-2017-175
Manuscript under review for journal Geosci. Model Dev.
Discussion started: 4 August 2017

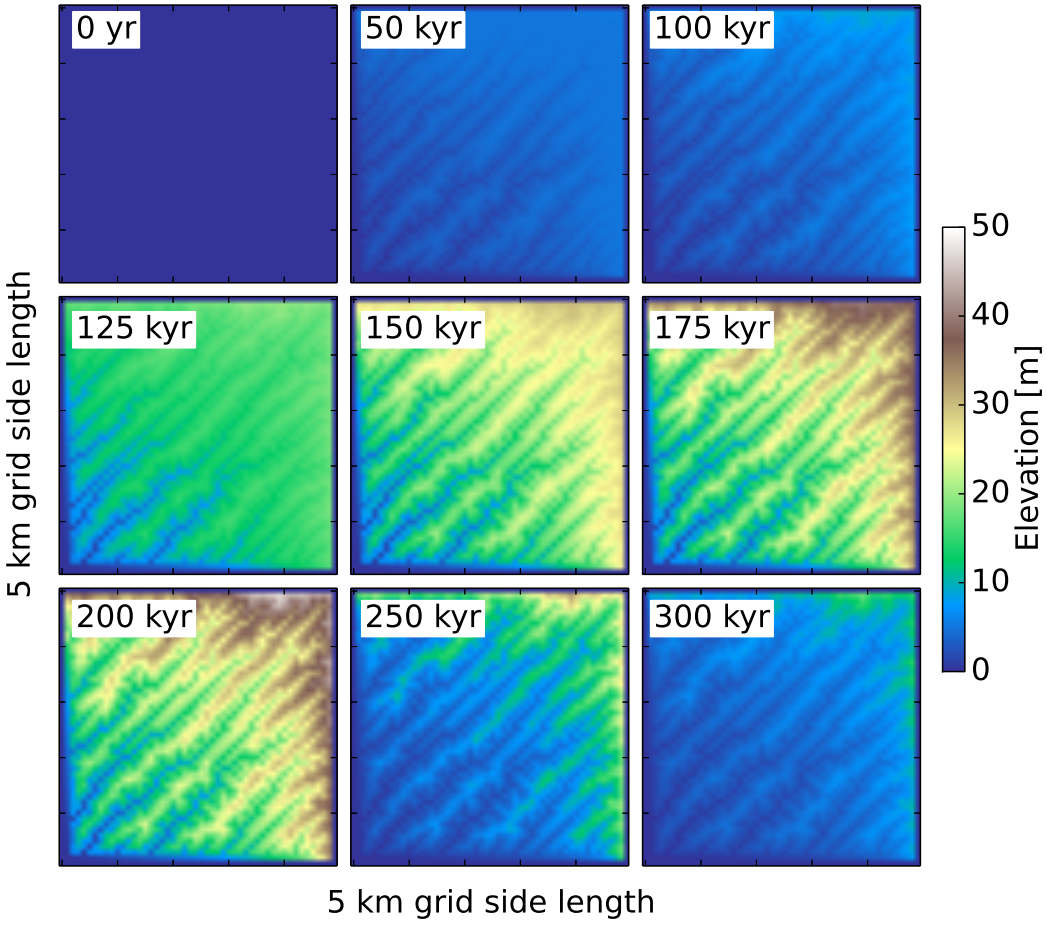

Figure 10. Snapshots of topography at nine times throughout the coupled SPACE and linear diffusion model experiment simulating the growth and decay of topography in response to changing rock uplift rates. The upper-left panel represents the model initial condition, a plane with initial micro-scale roughness slightly tilted towards the basin outlet. The outlet is located at the lower-left (southwest) corner of the model domain. The rock uplift rate is 0.0001 m/yr for the first 100 kyr, increases to 0.0005 m/yr for 100–200 kyr, then declines again to 0.0001 m/yr for 200-300 kyr. The model shows the growth of relief in response to rock uplift, with relief increasing slowly for the first 100 kyr and then more quickly for 100–200 kyr. After 200 kyr when the uplift rate declines to its initial value, relief declines as erosion of the high points on the landscape, driven by both fluvial erosion and linear diffusion, outpaces rock uplift.

Geosci. Model Dev. Discuss., https://doi.org/10.5194/gmd-2017-175
Manuscript under review for journal Geosci. Model Dev.
Discussion started: 4 August 2017

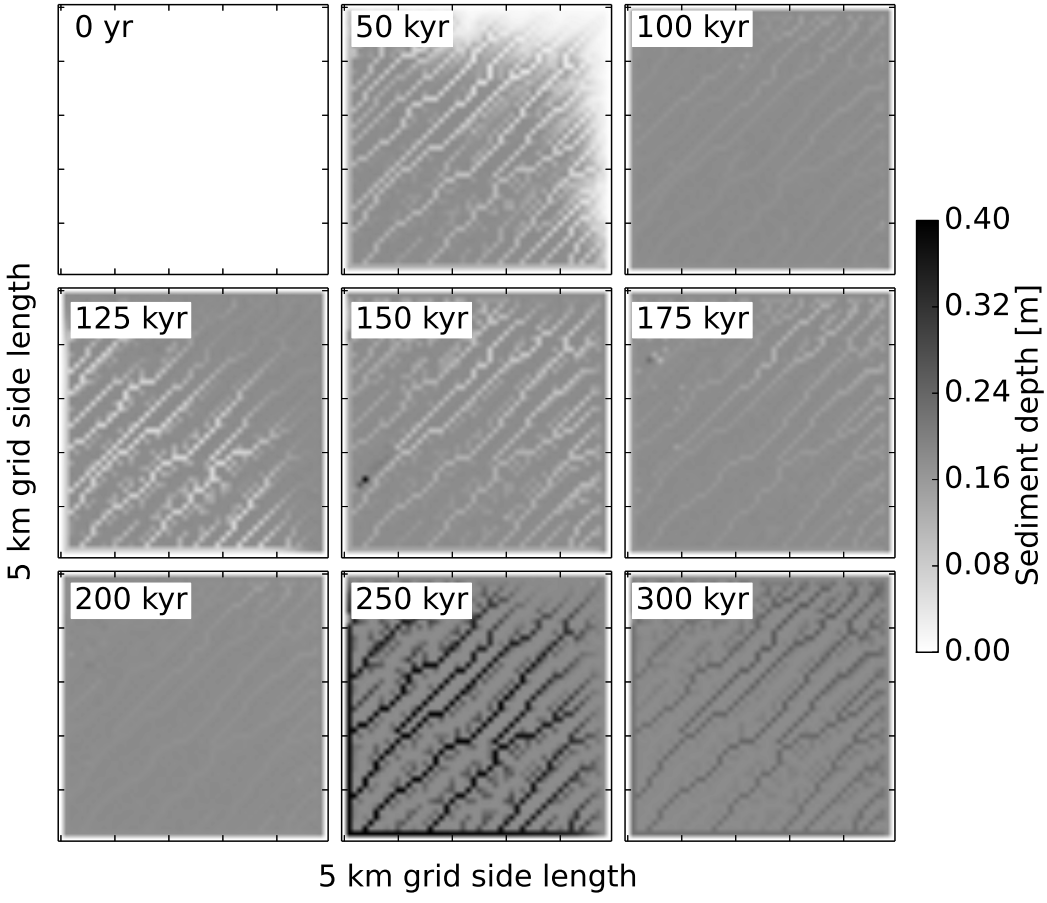

Figure 11. Snapshots of sediment thickness at nine times throughout the coupled SPACE and linear diffusion model experiment simulating the growth and decay of topography in response to changing rock uplift rates. The upper-left panel represents the model initial condition, a plane with initial micro-scale roughness slightly tilted towards the basin outlet. The outlet is located at the lower-left (southwest) corner of the model domain. The rock uplift rate is 0.0001 m/yr for the first 100 kyr, increases to 0.0005 m/yr for 100–200 kyr, then declines again to 0.0001 m/yr for 200-300 kyr. During the first 100 kyr, sediment depth increases on the hillslopes (because diffused material is considered sediment) but is absent in the channels as the channels incise into bedrock. By 100 kyr, the channels hold more sediment as incision and sediment thickness equilibrate to the rock uplift rate. As the rock uplift rate increases between 100 and 200 kyr, the same pattern occurs where sediment is evacuated from the channels during the initial response to rock uplift. The channels then re-alluviate as the landscape approaches equilibrium at 200 kyr. After 200 ky, the decline in rock uplift causes initial alluviation in the channels as diffusion into the channels outpaces sediment erosion. Finally, sediment thickness declines in the channels as the pace of diffusion slows in response to relief reduction.

Geosci. Model Dev. Discuss., https://doi.org/10.5194/gmd-2017-175
Manuscript under review for journal Geosci. Model Dev.
Discussion started: 4 August 2017

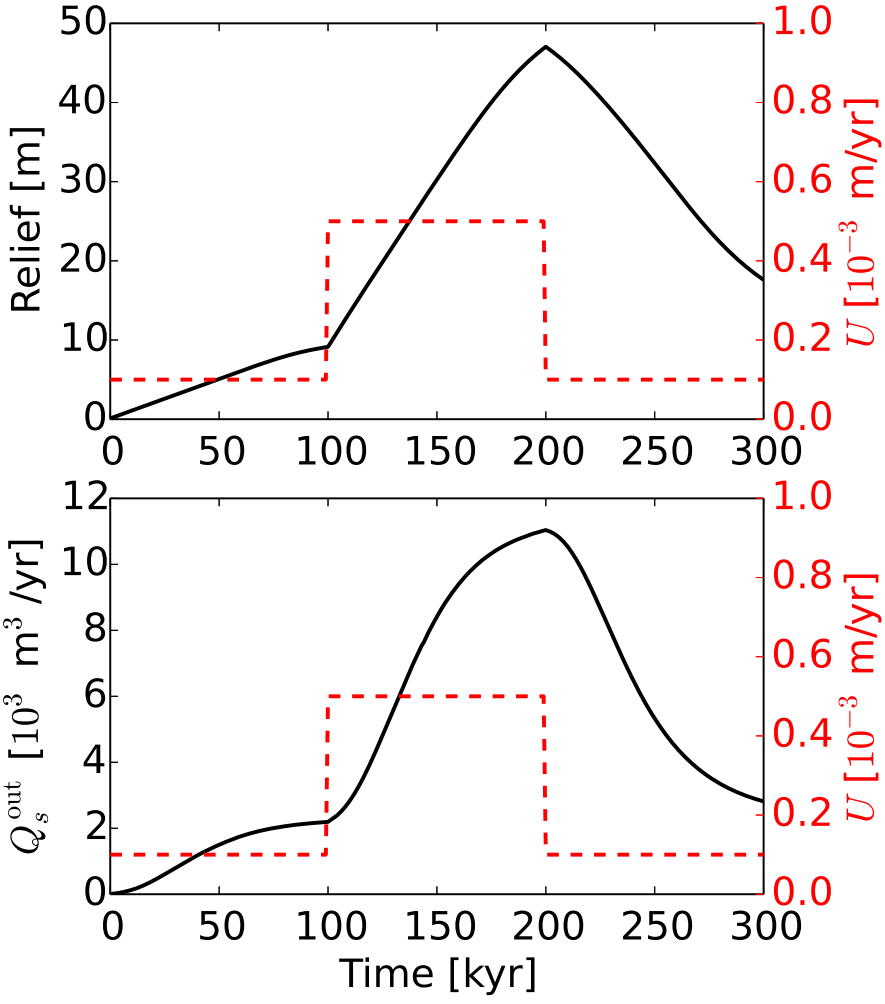

Figure 12. Time series of total relief in the model domain (top) and sediment flux out of the model domain (Q_s^{out}, bottom) shown with the imposed rock uplift rate U. Both relief and sediment flux increase slowly during the first 100 kyr in response to the imposed rock uplift rate of 0.0001 m/yr. By the end of the first 100 kyr, the rates of increase for both relief and sediment flux become slower, indicating that the landscape is approaching equilibrium with the rock uplift rate. Between 100 and 200 kyr, the rock uplift rate is increased by a factor of five and both relief and sediment flux increase by approximately the same factor. By the end of the 100 kyr period of high rock uplift rate, relief and sediment flux begin to equilibrate to the new, higher rock uplift rate. At 200 kyr, the rock uplift rate is reduced to its original value, and relief and sediment flux decline in response as erosion of high points on the topography outpaces rock uplift.